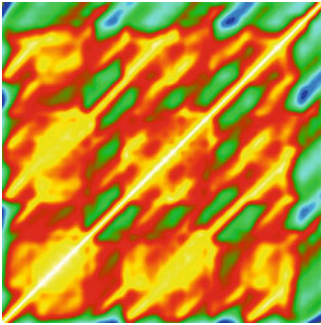


Chapter 10

Dynamical Patterns in Seismology

Tamaz Chelidze and Teimuraz Matcharashvili



Abstract Earthquakes are important components of complex dynamical Earth systems known as geocomplexity. One of the main contributors to geocomplexity is the seismic process which notoriously displays nonlinear behaviors including the self-organization of many interacting components (tectonic plates, faults). These processes result in seismic (macro-scale) events of collective behaviors in the temporal, spatial and energy domains. In the chapter the results of both active and passive experiments on triggering/synchronization are presented. The dynamic patterns of seismicity are revealed by the application of nonlinear dynamics tools to time series from: “laboratory” earthquakes (acoustic emission during natural stick-slip and stick-slip under weak periodic forcing), regional seismicity of the Caucasus Mountains, local seismicity in the area of large reservoir during its construction and regular exploitation, as well as from analysis of variations in local seismicity in a Central Asia test area due to application of strong electric pulses. The review of recent results on dynamic triggering of local seismicity by remote earthquakes is also presented. It is shown that relatively weak external forcings can induce clear changes in modeled and real earthquake dynamics. Recurrence Quantification Analysis (RQA) proved to be an efficient method for finding hidden nonlinear structures in seismic time series. Quoting Webber and Zbilut (2005): “. . . *whatever the case, whether it be forecasting dynamical events in the medical field, geophysics, or meteorology, the future of recurrence analysis looks bright and promising.*”

T. Chelidze (✉) • T. Matcharashvili
Institute of Geophysics, Tbilisi, Georgia
e-mail: tamaz.chelidze@gmail.com

10.1 Introduction

Earthquakes (EQs) are important components of complex dynamical Earth systems known as geocomplexity. One of the main contributors to geocomplexity is the seismic process which notoriously displays nonlinear behaviors including the self-organization of many interacting components (tectonic plates, faults). These processes result in seismic (macro-scale) events of collective behaviors in the temporal, spatial and energy domains. The attributes of complexity include critical phenomena, scaling properties, formation of time-space patterns, intermittency, and extreme sensitivity to initial conditions and weak forcings. This last chaotic property implies that the manifestation of seismic processes such as EQs can be triggered by relatively weak external forcings.

The Earth is dynamically subjected to oscillating force fields of differing origins (foci) over an extremely wide range of frequencies (periods of seconds to months to years). Since these oscillating forces are not isolated from the Earth's plates, they produce rhythmic stress/strain fields within the Earth's crust expressed as triggering and synchronization phenomena. This sensitivity to weak external forcings implies that the affected system is close to its critical state, where the sensitivity of the system to, weak impacts is very high.

Early observations of triggering/synchronization (T/S) were not validated by trustworthy field observations or strict mathematical procedures. Thus they should be considered as mainly qualitative if not unreliable. However, the situation has changed dramatically over the last decade with the implementation of dense seismic networks equipped by high sensitivity broadband devices. Now it is possible to identify reliable triggering events as spatially and temporally correlated local events following strong EQs. In the important domain of earthquake seismology where strong remote EQs trigger local seismicity patterns, experimental measurements trump mathematical theory.

Active laboratory experiments on the electromagnetic (EM) and mechanical triggering and synchronization of mechanical instability (slip) in the spring-slider system are herein considered in detail. In this case the main variables of the stick-slip (which is a small-scale model of seismic process) can be controlled. The forcing of local seismicity by periodic reservoir loading and strong electromagnetic pulses, wave trains from remote earthquakes can be considered as semi-active experiment where only some of process-determining variables are known. Lastly, analysis of seismic catalogs for revealing hidden periodicities represent passive experiments where most of key variables are unknown.

The robust theoretical analysis of T/S phenomena was also strongly facilitated by recent developments in the field of modern nonlinear dynamics which allows for quantitative interpretation of many of the mentioned unconditional effects. For relaxation (integrate and fire type) processes, when the signal is composed of well-defined marked events (slips, EQs), the generalized phase difference can be used for computing and comparing phases between events. Other possible measures for quantification of synchronization include Recurrence Quantification

Analysis (RQA), mutual information (MI), Shannon and Tsallis entropies, conditional probability of phases, flatness of stripes of synchrograms (stroboscopic approach), coefficients of phase diffusion, fractal dimension, Lempel–Ziv complexity, and unstable periodic orbits. For revealing hidden periodicities in short and noisy time series, which can be related to synchronization effects, the methods of Singular Spectral Analysis (SSA) and Detrended Fluctuation Analysis (DFA) have been suggested [1, 2]. Lastly, in the case of very restricted statistics (tens of events), less demanding methods such as Shuster test can be used.

From the famous “butterfly effect” of Edward Lorenz we ask the question: Can weak external forcings trigger or synchronize seismic processes which are driven by enormous tectonic forces? It is accepted [3] that the Earth’s lithosphere has active seismic regions close to their critical state which means that even weak impacts can trigger massive EQs. Many experimental observations confirm the possibility that significant events can be elicited by a wide variety of small impact forces: coulomb stress changes induced by previous strong EQs [4]; mining activity and water reservoir loadings [5, 6]; nuclear explosions [7]; snow melts [8]; strong electrical pulses [9, 10]; tides [11, 12]; wave trains of strong EQs [12–15]; solar activity; atmospheric pressure and magnetic field variations.

Nonlinear dynamics provides a solid theoretical basis for explaining observed unconventional results [16–22]. New tools for quantification of the strength of T/S between the phases of synchronized process and synchronizing impact have been developed over the last years making the corresponding assessments much more reliable [23].

Analysis of the susceptibility of the region’s seismic process to a small impact may serve as a new method of EQ prediction. This idea is founded on the hypothesis that closer is the system to the critical state, the stronger is its sensitivity to small forcings [24]. Application of nonlinear dynamics to time series related to various catastrophic phenomena reveals striking universality in the precursory patterns of such different events as seismic shocks, financial crises, cardiac attacks and epileptic seizures [25, 26].

The physical modeling of seismic T/S phenomenon is not well developed. In particular there are problems related to driving/forcing stress amplitudes and periods, the role of fluids, inhomogeneities, etc. that favor/suppress triggering.

10.2 Elements of Seismology

10.2.1 *Physics of Earthquakes*

Earthquakes (EQ) constitute important components of complex dynamical Earth systems. They are caused by the slow drift (1–8 cm/year) of Earth’s lithosphere plates driven by thermal convection in the underlying molten asthenosphere. EQs represent one of the main expressions of the release of stress which accumulates

due to this motion [3, 27]. Non-EQ manifestation of stress build-up is slow creep (several mm/year). As a rule EQs occur on active faults delineating the borders between lithosphere plates and smaller blocks. Main variables characterizing EQs include: magnitude (logarithmic measure of EQ size or energy); location; depth and timing. Bak et al. [28] considered seismicity as a self-organized process.

10.2.2 Stick-Slip as a Physical Model of the Seismic Process

Seismicity is considered as a nonlinear frictional process of the “integrate and fire” type. Here shear stresses build up (integrate) on the fault plane until the friction force is exceeded. This leads to a sudden drop in stress (fire) after which a new epoch of build-up begins again. Hence the process is non-periodic cyclic [27]. This recurrent stick-slip process can be modeled both theoretically and experimentally by single or multiple spring-slider systems.

10.2.3 Seismic Time Series

Seismic time series represent continuous recordings of Earth’s surface weak vibrations or microseisms with relatively rare strong events (EQs). Seismic catalogs are data tables containing information of the main characteristics of EQs (date, location and magnitude) and organized according to the date of events. Declustered from foreshocks and aftershocks, strong events in EQ catalogs are mainly Poisson distributed. Several methods of synthetic seismic catalog compilation have been suggested. One good example is the Epidemic-type aftershock sequence model [29] which produces results mimicking those found in natural EQ catalogs.

10.2.4 Scaling Relations

In 1954 the observation was made that scaling relationship existed between EQ frequency and EQ magnitude. This was known as the Gutenberg–Richter law (G–R law), one of the first fractal laws. The G–R law states that: $\log N = a - bM_s$, where M_s is the surface wave magnitude, N is the annual frequency of EQs, and a and b are regional constants. In general it has been shown that power law distribution pointing to self-similarity or scale invariance holds in EQ magnitude, temporal and spatial patterns. It should be noted that as a rule the strongest EQs follow special distributions (e.g. Gumbel probability density function) for extreme events.

10.2.5 Patterns of Seismicity

Different models have been developed to describe the statistical properties of EQ distributions in time, space and magnitude domains [30]. According to one model, strong EQ events on a given fault line occur quasi-periodically. A second model assumes that EQs occur independently and follow the Poisson distribution (i.e. seismic events are randomly distributed). Recent results indicate that some complex seismic processes have patterns of nonrandom dynamical structuring [31–33]. For example, Matcharashvili et al. [32] showed that the qualitative and quantitative analysis of sequences of EQ magnitude and waiting times in the Caucasus Mountains showed evidence of being low-dimensional and nonlinear. This result was similar to the findings of Goltz [31] for the temporal distribution of Japanese EQs (1997). Then Sobolev [34] reported existence of deterministic chaos in (smoothed) seismic time series. In any case the disagreements are substantial enough to preclude concluding that the real seismic possess possesses dynamical patterns that are strictly deterministic or completely random. Many intermediary possibilities exist.

10.2.6 Earthquake Prediction

Opinions vary on the possibility of predicting EQs from the mainly positive arguments [35–37] to the strongly negative arguments [38]. EQ prediction is a major challenge to Earth sciences and implies assessment of three main characteristics of impending EQ: location; magnitude and time of occurrence. The assessment of prediction success is an object of complex statistical evaluations [39, 40]. The problem seems intractable since even if the first two characteristics (location and magnitude) are more or less well forecasted using geological, historical and instrumental data, prediction of the timing of strong events still evades prediction. Application of modern methods from nonlinear dynamics allow for the revealing new fine structures in geophysical time series which might be useful for finding predictors of strong events [41]. One positive observation is that the waiting times of EQs possess the property of low-dimensionality/memory. On the negative side, prediction of EQ magnitudes should be much more difficult due to the high dimensionality of their distributions [32].

10.2.7 Earthquake “Control”

Experiments show that relatively weak forces, such as reservoir exploitation, mining, water injection in wells, etc., can affect dynamical features of seismic processes. Such effects are sometimes understood as T/S processes or seismic

activity controls [5, 6, 42, 43]. Investigations are still underway, but so far the control of seismicity by weak forcings resides more in the domain of science fiction than science fact. This is not to say that positive outcomes may not be realized in the future [44]. The phenomenon of triggering and synchronization of local seismicity by the wave trains generated from remote earthquakes can be mentioned as an interesting related effect [13, 45]. Such views on possible EQ control are supported by recent discoveries on behavior of complex systems under external influences. Phase and coherence synchronization phenomena are examples of such effects [23, 46, 47]. Indeed as in any complex system, depending on the conditions (parameter settings) weak forcings may exert a control effect as happens with chaotic oscillators driven by a series of weak impacts. In this last case a chaotic attractor containing an infinite number of unstable periodic orbits can be stabilized by a tiny perturbation of system many orders of magnitude less than the main driving force [48, 49]. The control can even be achieved by non-persistent (single pulse) perturbations [50].

10.3 Methods of Revealing Dynamic Patterns in Acoustic/Seismic Time Series

It seems informative to consider the relationship of T/S phenomena to such concepts as ordering, control, self-organization, coupling of systems, randomness and determinism. The phenomenon of triggering is related to the coupling of two dynamical systems in which one is driven by a relatively strong force and the second one by a relatively weak force. Still this small impact introduces significant nonrandom (isolated) action in the former system (e.g. triggered discharge). Synchronization, on the other hand is related to a fundamental property of dynamical systems, specifically their recurrence. Synchronization can be considered as a specific kind of ordering in a series of data, namely, regular recurrence of some characteristic events caused by coupling of two or more systems in master and slave manner. Coupling of even decentralized dynamical systems can lead to self-organization phenomenon (like coherent flashing of firefly swarms), which can be also considered as self-synchronization of oscillators possessing different properties.

There are several kinds of synchronization between oscillating autonomous systems each with a natural frequency (ω_0) and forcing frequency (ω): partial; strong and weak; imperfect (non-locking); generalized (strong coupling with tight functional correlation); complete (nearly identical oscillations in two systems); and phase synchronization (PS). If the amplitudes are irregular and uncorrelated, but the forcing frequency ω and resulting frequency of forced system Ω are adjusted, there is a regular phase shift between ω and Ω . An interesting effect is a high-order or ($n:m$) synchronization, when observed Ω and forcing frequencies ω satisfy equation [23]: $n \omega = m \Omega$, where n and m are integer numbers. The ratio n/m is called the winding or rotation number ρ and is defined as: $\rho = \Omega/\omega$ or in terms of the oscillators' phases: $|n\phi - m\phi_{obs}| < const$, where ϕ is the phase of the forcing and ϕ_{obs} is that of the kicked oscillator.

There are several main approaches to quantify the complexity/synchronization of processes by analysis of measured time series [23, 33, 51]. Some approaches are rooted in dynamical systems theory and fractals and include Lyapunov exponents and fractal dimensions (i.e. correlation dimensions). These methods are based on reconstruction and testing of objects having phase spaces equivalent to the unknown dynamics. The possible calculated measures for quantification of synchronization are: generalized phase difference; mutual information [52]; first Fourier mode of distribution of relative phases; conditional probability of phases [53]; flatness of stripes of synchrograms or stroboscopic technique [54]; and coefficients of phase diffusion [55]. We suppose that analysis of unstable periodic orbits can also be used to reveal synchronization and ordering in coupled time series [44]. The other methods stem from the information theory including Shannon or Tsallis entropy [56], algorithmic complexity [57], etc. It should be stressed that both laboratory stick-slip and EQ source evolution can be considered as the relaxation (integrate and fire type) processes, where the acoustic/seismic signals contain well-defined marked events corresponding to slips/EQs. To deal with relatively short time series new tests have been proposed such as recurrence plots (RP) and recurrence quantitative analysis (RQA). In the case of very restricted statistics (tens of events) less demanding methods, such as Shuster test [58] can be used.

Here we provide a cursory overview of methods. More detailed descriptions can be found in many other sources (e.g. [59–68]).

The term recurrence plot was introduced by Eckmann et al. [60]. The RP construction method was inspired by the fact that nonrandom dynamical systems are characterized by returns to specific state-space locations. Thus recurrence is a fundamental property of any deterministic dynamical system. Recurrence properties also hold for systems which are not exactly deterministic but have nonrandom dynamical structures. Generally, recurrence properties of such systems are stronger if their behavior in the phase space is close to a so-called deterministic dynamical structure (attractor). RPs graphically visualize moments when two trajectories visit the same region in phase space. It is at these points when the system displays recurrences.

According to Eckmann et al. [60] the RP can be mathematically expressed as:

$$R_{i,j}(\varepsilon) = \Theta\left(\varepsilon - \left\| \vec{x}_i - \vec{x}_j \right\| \right) \quad i, j = 1, \dots, N \quad (10.1)$$

where N is the number of measured x_i points. Phase space vectors \vec{x}_i are higher-dimensional reconstructions from measured one-dimensional observations by applying Takens' time-delay method. Each vector of the reconstructed phase-space trajectory is tested for proximity to another vector of the trajectory by testing whether the distance between them is less than a specified threshold ε (radius). Finding of reliable threshold value is not an easy task as has been much discussed in various publications (e.g. [61, 64, 69, 70]). Generally it is reasonable to recognize that the selection of the recurrence threshold is neither straightforward nor optimal. Indeed, radius choice really depends on the particular problem and data set at

hand [70]. It is not necessary to repeat these well-known views about threshold calculation, but for the purposes of this chapter a threshold was typically set to 20 % of the mean of all distances in the distance matrix and l_{min} was set to 2–4 as recommended by others [66, 71].

According to Eq. (10.1), the recurrence matrix contains elements of 0 values (non-recurrent vectors) or 1 values (recurrent vectors). The square recurrence matrix is easily visualized by plotting elements i vs. j as black points if $R_{i,j} = 1$ or white points if $R_{i,j} = 0$. Since i and j are both functions of time, time travels up the ubiquitous line of identity where $R_{i,j} = R_{i,j} = 1$ (always recurrent by self-identity). The main advantage of the RP approach is that it enables the two-dimensional visualization of the recurrence matrix projected from higher-dimensional phase-space trajectories.

As beautiful as RPs appear, the evaluation of the RPs remains a visualization task or qualitative art. For this reason RQA was developed in order to quantify differently appearing RPs based on the small-scale structures contained therein. As a quantitative extension of the RP methodology, RQA can be used as a tool for studying the temporal dynamics of a complex time series. RQA was introduced by Zbilut and Webber [61], Webber and Zbilut [72]. This technique quantified visual features in an $N \times N$ distance matrix recurrence plot and defined five measures of complexity based on diagonal line structures in the recurrence plot: recurrence rate (%RR), determinism (%DET), maximum diagonal line length (DMAX), entropy (ENT) and trend (TND). Three of these variables were used in the present research (%RR, %DET, ENT).

By definition %RR is the ratio of number of all recurrent states (recurrence points) to the number of all possible states and is therefore the recurrence probability of a certain state. There exists a scaling relationship between %RR and the radius which mimicks the correlation dimension [63]. That is why it is crucial to keep the radius parameter low so as not to saturate the RP with recurrence points which are in fact distant from one another. %DET is the ratio of the number of recurrence points forming diagonal structures to the total number of recurrence points in the RP. Specifically, %DET is the proportion of recurrence points forming diagonal structures of a length l_{min} or greater. Periodic systems (e.g. sine waves) inscribe long diagonals and are highly deterministic. Conversely, chaotic signals produce very short diagonals, yet these systems are fully deterministic. Stochastic signals or wildly fluctuating (transient) data produce no diagonals or only short diagonals (only per chance). ENT is the Shannon entropy computed from the histogram distribution of diagonal line lengths of length l_{min} or longer. ENT measures the complexity of the dynamical system under scrutiny.

Over a decade later Marwan extended the RQA approach by introducing three additional measures including, laminarity (%LAM), maximum vertical line length (VMAX) and trapping time (TT). These variables describe characteristics of the vertical line structures in RPs [66]. %LAM is defined as the fraction of recurrent points forming vertical lines with a length of l_0 or greater. This measure is related to the density of laminar states in the system because a vertical/horizontal line marks a length of period in which a state does not change or changes very slowly. Then

TT is defined as the average length of the vertical lines as contrasted with VMAX which registers just the longest vertical line structure. Two of these variables were used in the present research (%LAM, TT).

For interpretation purposes, it is assumed that the quantification of diagonal structures by RQA is able to reveal transitions between ordered and disordered states of a system. Alternatively, RQA measures based on vertical (horizontal) structures are more suitable to identify transitions between different disordered conditions.

Beside the difficulty of setting the radius, at least two additional parameters must be selected before RQA can commence. The delay time is best estimated by submitting the test signal to mutual information (MI) analysis. The embedding dimension is best estimated by the false nearest neighbors (FNN) approach.

To conclude this short overview we note that RQA does not require that the input data (time series) be of any particular distribution, be stationary, be noise free, or be particularly long. In fact, input data can contain as few as 30 points. These characteristics of RQA make it a powerful tool when dealing with real-world data sets [63, 66].

10.4 Triggering and Synchronization of Stick-Slip: Laboratory Model of Seismic Process

In this review the results of both active and passive experiments on T/S are presented. In the case of active (laboratory) experiments on the electromagnetic (EM) and mechanical triggering and synchronization of mechanical instability (slip) in the spring-slider system, the main variables of the stick-slip (which is a small-scale model of seismic process) can be controlled. The forcing of local seismicity by periodic reservoir loading, strong electromagnetic pulses and wave trains from remote earthquakes can be considered as semi-active experiments where only some of process-determining variables are known. Lastly, the analysis of seismic catalogs for revealing hidden periodicities is a passive approach in which key characteristics of the process are mostly unknown.

Many publications over the last decades have addressed EQ triggering (especially dynamic triggering), but the problem is far from being resolved due to the complexity of natural seismic processes [3, 11, 13, 19, 27, 73]. We believe that a reasonable understanding of the T/S phenomena can best be obtained from controlled experiments carried out on model systems [24, 74–78]. It is generally accepted that the most relevant model of the seismic process is unstable frictional movement or stick-slip [79–81]. This is a special case of the relaxation, integrate and fire model. In our stick-slip experiments, acoustic emissions (AE) signaling slip events and electromechanical (EM) or mechanical forcings were recorded on two separate channels of a sound card (Figs. 10.1, 10.2, 10.3, 10.8a, 10.9a, and 10.10).

Laboratory experiments were carried out on the slider-spring system with superimposed pulse or periodic electromagnetic (EM) or mechanical forcing both of which are weak compared with the main dragging force of the spring. The

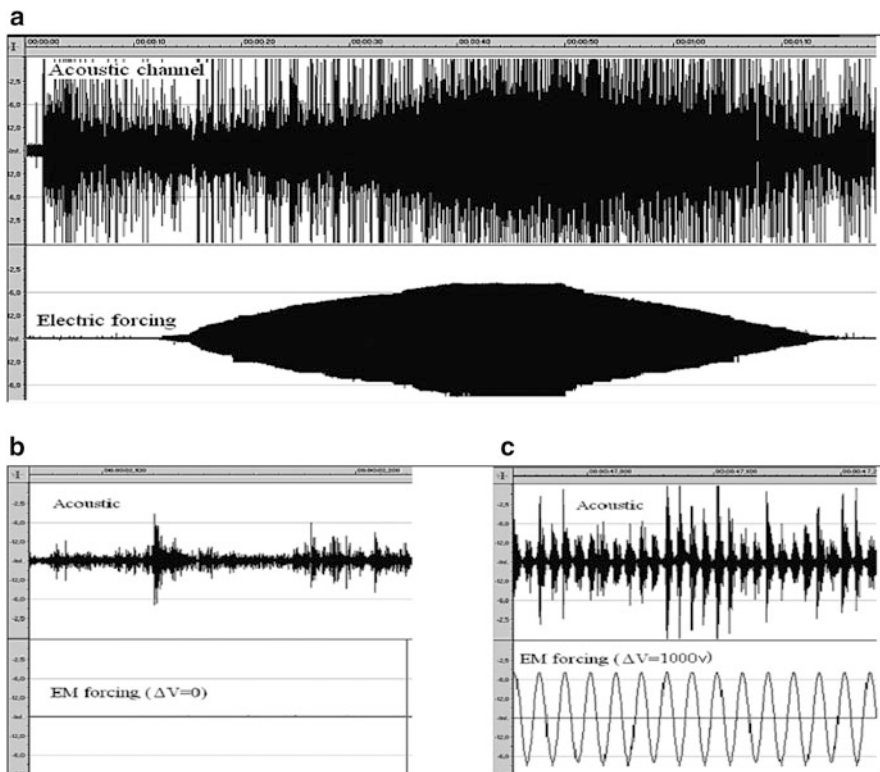


Fig. 10.1 (a) Acoustic emission during slip under variable from zero to 1,000 V external periodical voltage. (b) The extended part of record with zero EM forcing. (c) The extended middle part of record under maximal EM forcing with complete phase synchronization (PS)

details of experimental setups can be found elsewhere [83, 84]. Relative forcing (RF) or coupling strength was calculated as a ratio of the forcing intensity to the main driving force. In our laboratory experiments RF was of the order of 10^{-2} with EM forcings and of the order of 10^{-3} – 10^{-5} with mechanical forcings. For selecting AE signals from the noisy records we use an approach modified from Akaike Information Criterion (AIC), which gives good coincidence with manual selections.

10.4.1 Electromagnetic Triggering of Slip

The first set of triggering experiments was prompted by experiments carried out from 1983 to 1988 by the Institute of High Temperatures (Russia) at the Bishkek test area. After performing a series of MHD soundings as well as “cold” discharges,

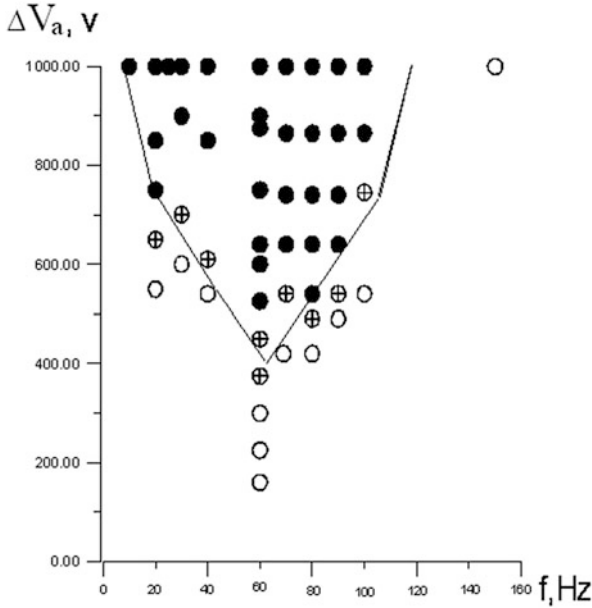


Fig. 10.2 Stick-slip synchronization area (Arnold's tongue) for various intensities (V_a) and frequencies (f) of the external EM forcing. *Filled circles*: perfect synchronization; *circles with crosses*: intermittent synchronization; and *empty circles*: absence of synchronization [82]

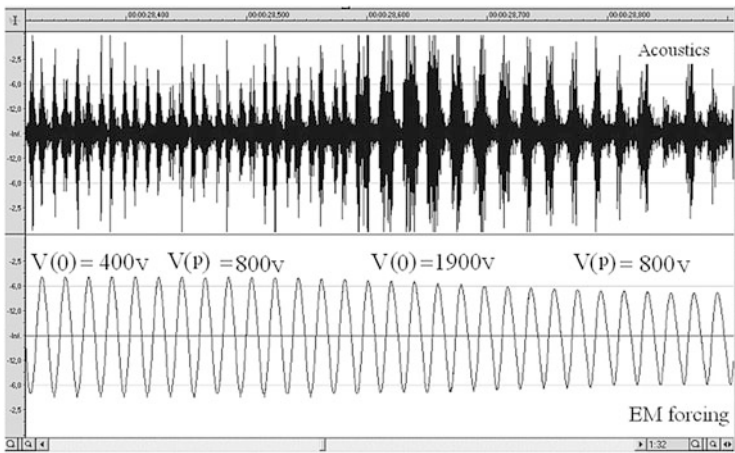


Fig. 10.3 Transition (bifurcation) in stick-slip from 1:2 synchronization (period doubling) to 1:1 synchronization at simultaneous action of direct $V(0)$ and periodic $V(p)$ voltages; transition occur at $V(0) > V(p)$ [82]

an unexpected effect of micro-seismicity activation by strong EM pulses was discovered [9, 10]. We modeled this effect using a rock block placed on the inclined fixed block at the angle less than the critical repose angle. At this angle the system was stable (non-moving) for days. Application of strong electromagnetic (EM) pulses initiated (with some probability) mechanical instability (slip) provided the electrostriction force parallel to the slip surface. On the contrary, slip was hampered if the EM field was applied normal to the surface. The EM field contribution F_{pi} to the friction force F_f can be written as:

$$F_f = \mu (F_n + F_{pi}), \quad (10.2)$$

where μ is friction coefficient, F_n is normal force including pore pressure contribution and F_{pi} is electrostriction force acting in the gap between blocks' contacting surfaces. Using known expression for electrostriction force [85] we obtain:

$$\vec{F}_{pi} = \pm \frac{\varepsilon_{eff} S}{8\pi} \left(\frac{\Delta V_{eff}}{d_{eff}} \right)^2 \vec{n}, \quad (10.3)$$

where $\Delta V_{eff}/d_{eff}$ is the effective voltage gradient in the gap, ε_{eff} is the effective dielectric constant of the gap and S is the area of the slip surface. The positive sign (+) is applied when the EM field \vec{E} is parallel to the external normal \vec{n} to the surface and the negative sign (−) when the field \vec{E} is normal to \vec{n} [77].

It is remarkable that the expression (10.2) is similar to Byerlee's friction law which takes into account fluid pore pressure contribution to the friction force [86]. A significant difference is that additional EM force can be positive or negative.

10.4.2 Electromagnetic Stick-Slip Synchronization

Synchronization experiments with electromagnetic (EM) forcings were carried out on the system consisting of two (horizontal) plates of roughly finished basalt. A constant pulling force F_p of the order of 10 N was applied to the upper (sliding) plate. In addition, the same plate was subjected to periodic electric forcing of variable frequency and amplitude (from 0 to 1,000 V) which was mechanically much weaker (of order of 1 N) compared to the pulling force. The electric field was normal to the sliding plane. Acoustic bursts accompanying slip events were registered by the PC sound card. Details of the setup and technique are previously published [84].

Acoustic emissions during slip with superimposed periodic low-frequency EM field ($f \approx 60$ Hz) of varying intensity, oriented normally to the slip surface are presented in Fig. 10.1 [82]. The significant synchronization at this frequency occurs at $V_a \geq 500$ V. At such conditions excitation the AE events (micro slips) is synchronized with EM field and occur twice per period (Fig. 10.1C).

Synchronization was observed only at some definite values of set of parameters (spring stiffness K_s , frequency f and intensity V_a of forcing). The “phase diagram” for variables f and V_a or so-called Arnold’s tongue [23] is presented in the Fig. 10.2.

It should be noted that the phenomenon of synchronization was observed only with the EM field directed normally to the slip surface. When the EM field was applied roughly parallel to the slip plane, synchronization was absent. We conclude that the synchronization is related to “electromagnetic braking” of slip at large enough values of (normal) sinusoidal EM forcing (large positive EM field contribution F_{pi} in Eq. 10.2) and a sudden slip after accumulation of critical stress provided by spring pull (as was noted in the previous section, the effect of EM “braking” was discovered in slip experiments on the inclined slope).

Also observed is a transition (bifurcation) in stick-slip from 1:2 or period doubling synchronization when two slip events occur per period of EM forcing to 1:1 synchronization when one slip event occur per period of EM forcing (Fig. 10.3). At simultaneous action of direct $V(0)$ and periodic $V(p)$ voltages the transition occur at $V(0) > V(p)$. A simple explanation of the period doubling effect follows from the principle of electrostriction in which direct and periodic voltages are simultaneously applied to a dielectric material [77].

10.4.3 Measuring EM Synchronization Strength of Stick-Slip

Several quantitative analysis tools were applied to the recordings of stick-slip processes where the superimposed periodic EM field intensity was raised monotonously from zero to 1,000 V and then decreased back to zero (Fig. 10.1a). In order to assess synchronization in a quantitative manner various tools of nonlinear dynamics (synchronization) theory described in [18, 23, 64, 87] were applied to experimental data (Fig. 10.1a) obtained under variable intensity of forcing. Specifically, we calculated: phase difference $\Delta\Phi$ between acoustic emission bursts and external sinusoidal forcings; phase diffusion coefficient D of phase differences $\Delta\Phi$; mutual information (MI) between phase of forcings and AE bursts and recurrence plots (RP) and RQA %DET measures of stick-slip generated AE time series. The results are shown in Figs. 10.4, 10.5, 10.6, and 10.7. All these methods confirm strong synchronization of forcing and AE at maximal EM forcing.

10.4.3.1 High Order EM Synchronization of Stick-Slip

High-order or ($n:m$) synchronization means that observed T_{obs} and forcing T_f periods of oscillators satisfy equation [23]: $nT_{obs} = mT_f$, where n and m are some integer numbers. The ratio n/m is called the winding or rotation number ρ and is defined as:

$$\rho = T_f / T_{obs}. \quad (10.4)$$

Fig. 10.4 Phase difference $\Delta\Phi$ between the sequence of maximums of acoustic emissions' bursts (AE catalogue) and external sinusoidal EM forcing versus time for a whole record, Fig. 10.1a. Note that $\Delta\Phi$ remains practically constant at forcings stronger than the threshold value of V

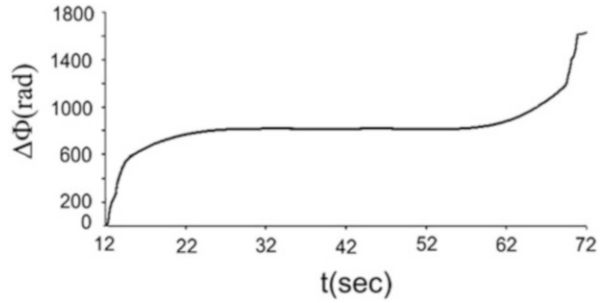


Fig. 10.5 Variation of phase diffusion coefficient D of phase differences $\Delta\Phi$ versus time, calculated for consecutive sliding windows, containing 500 events for data presented in Fig. 10.1a—for a whole record. Note that D remains rather constant near zero at the forcings stronger than the threshold value of V

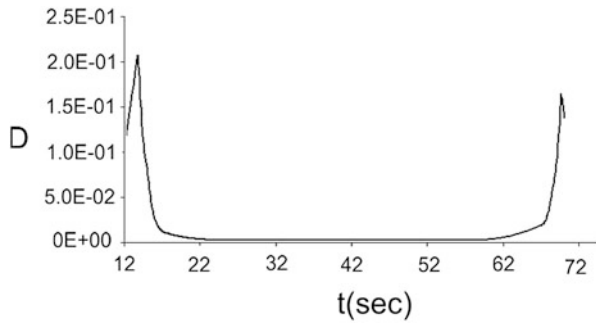
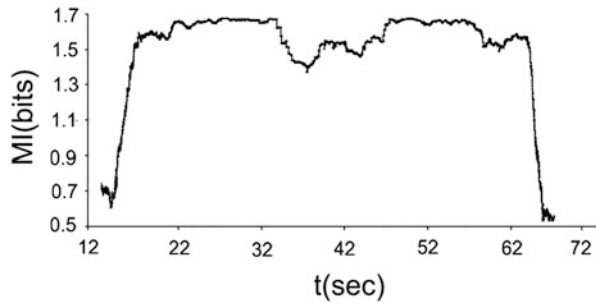


Fig. 10.6 Variation of mutual information between the phase of forcing and AE bursts versus time calculated for consecutive sliding windows, containing 500 events (for a whole record presented in Fig. 10.1a). *Note:* large values of MI in the same range of t , where $\Delta\Phi$ is constant and D is very small



This condition of high-order synchronization can also be presented as a ratio $n:m$; in this case the winding number is: $\rho = n/m$.

The experiments [77, 89] show that the addition of a strong enough component of the constant electric field to the high frequency EM forcing signal (40 Hz) invokes transition from 1:2 to 1:1 synchronization. Figure 10.8 represents an example of high order ($n/m = 1:2$) synchronization as well as the high-order synchronization (HOS) of stick-slip at EM forcing by alternating pulses of different duration.

Both the onsets of AE swarms and those of the individual events within swarm sequences turn out to be very well organized which is evident from the synchrograms (Fig. 10.8b, c). The synchrogram (stroboscopic plot) implies a fixing of the phase of forcing EM signal at the moments of spiking of the acoustic pulses [23]. If the moments of n th spiking in the swarm ($n = 1, 2, 3$, etc.) always occur at

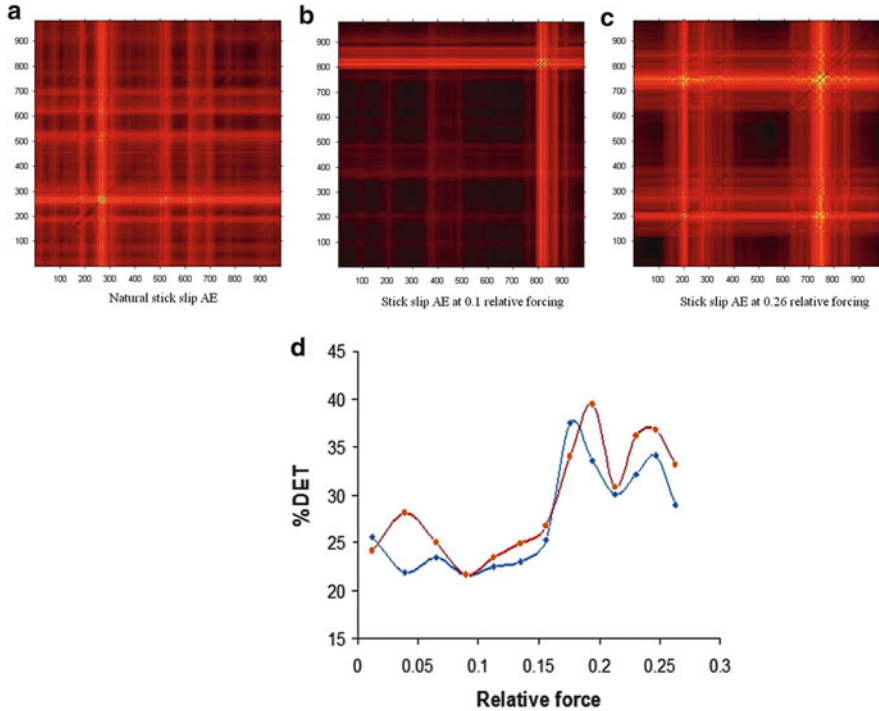


Fig. 10.7 Recurrence plots compiled using VRA program [88]; (a) RP of natural stick-slip. (b) RP of stick-slip at the relative forcing $RF = 0.1$. (c) RP of stick-slip at the relative forcing $RF = 0.26$; (d) %DET versus relative force (RF), calculated for onsets (red) and maximums (blue) of AE bursts for the first half of the record presented in Fig. 10.1a

the definite phase of the forcing, then both oscillators are synchronized and the plot of delays of n th spike relative to the onset of the forcing signal versus time (here the number of cycle for a periodic forcing) reveals n stripes parallel to the time axis. In Fig. 10.8b the synchrogram for the onsets of swarms of AE bursts and sequential AE signals within swarms generated during forcing by short EM pulses corresponds to the winding number $\rho = n:m = 1/3$. In the case of longer forcing pulses, $\rho = 1/4$ or $1/5$.

Figure 10.9a presents even more populated AE swarms generated by longer EM pulses. In this case the swarms contain up to 40 AE events, so $\rho = n:m \approx 1/40$. Again, the AE bursts within the swarm are surprisingly well organized. The corresponding synchrogram (Fig. 10.9b) shows that the first ten AE bursts show almost constant phase shift relative to the EM forcing onsets. The following bursts demonstrate regular small increase of the phase delay in sequential swarms [82]. It is striking how Fig. 10.9a, b are similar to synchronization pattern of neuron spiking under LF external electrical forcing ([23], Fig. 6.7). This constitutes a vivid illustration of universality of synchronization phenomenon.

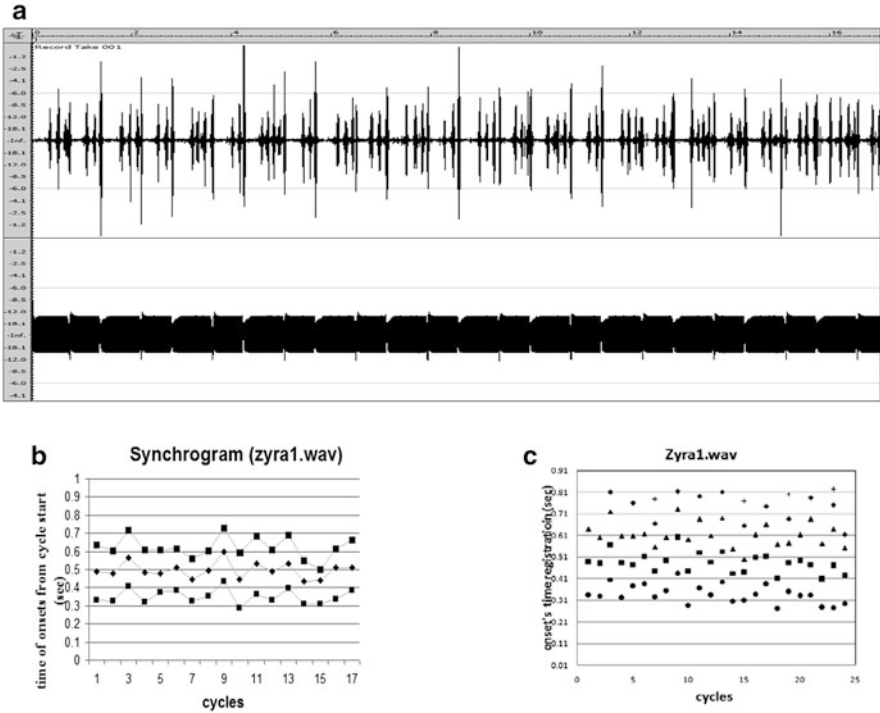


Fig. 10.8 (a) High order synchronization: $n < m$ (exp. Zyra1). Note that the onsets of slip swarms and these of the individual events within sequences (swarms) turn out to be very well organized (see text). (b) Synchrogram for the onsets of swarms of AE bursts and AE signals within swarms generated during forcing by short EM pulses versus number of forcing pulses (cycles), here $n:m = 1/3$. (c) A similar synchrogram for longer forcing pulses where $n:m = 1/4$ or $1/5$. *Note:* in this figure and Fig. 10.9 the LF forcing pulses are visualized by high-frequency (HF) modulation as the sound card does not respond to the direct current; HF is applied only to the computer channel (not to the sample)

10.4.4 Dynamic Mechanical Synchronization of Stick-Slip

Synchronization of the spring-slider system under weak periodic mechanical forcing has been investigated [77, 78, 90]. These experiments can be considered as laboratory modeling of the recently discovered effect of dynamical triggering/synchronization of local seismicity by the wave trains of strong remote EQs (Sect. 10.5.2). Two modes of mechanical forcing experiments were tested: (1) the forcing normal to the slip surface; and (2) the forcing parallel to the slip surface. For brevity we will refer to them as normal and tangential forcing accordingly. We calculated the maximum value of mechanical forcing which corresponds to the maximum measured voltage applied to the mechanical vibrator (i.e. when the voltage applied to the vibrator equals 6.5 V). The mass of the oscillating

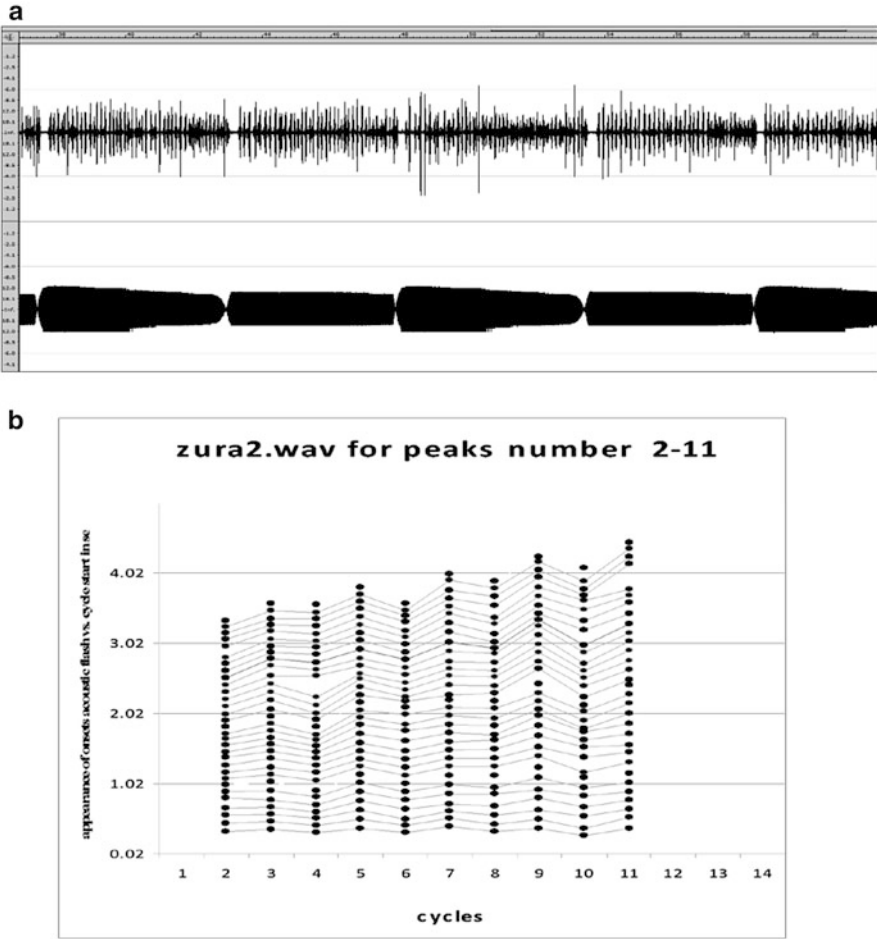


Fig. 10.9 High order synchronization: $n:m \approx 1/40$ (exp. Zura2). **(a)** Swarms of AE pulses (slips) generated during forcing by very long EM pulses. **(b)** Stroboscopic diagram (synchrogram) for the first 31 AE bursts in the swarms generated by 11 forcing EM pulses; note the stripe structure of synchrogram, which shows that the phase shift between onsets of electromagnetic (EM) forcing and acoustic emission (AE) pulses is almost constant for the first ten slips in the swarm [82]

element of the vibrator m is ≈ 20 g, so we obtain for the natural frequency f of the vibrator's oscillating element: $f = \sqrt{k/m} = 5$ Hz where k is the stiffness of the vibrator spring. Substituting into expression for maximal force $F_{max} = k x_{max}$ values of $k = 25$ and $m = 0.5$ N/m and that of the maximum deflection x_{max} of the oscillating element at the applied voltage 6.5 V (here $x_{max} \approx 4 \times 10^{-3}$ m), we obtain for the corresponding (maximal) intensity of mechanical forcing F_{max} : $F_{max} = k x_{max} \approx 2 \times 10^{-3}$ N.

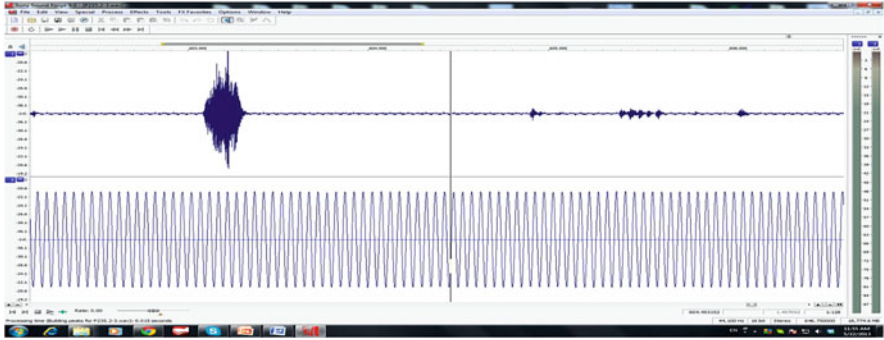


Fig. 10.10 Typical record of AE (*upper channel*) and simultaneous tangential mechanical forcing (*lower channel*). This example corresponds to vibration intensity generated by application of 5 V voltage to the vibrator. The *arrow head* demark the onset of slip (AE pulse). In the right part of record AE signals arise spontaneously without impulsive onsets and are analogs of non-volcanic tremors (see Sect. 10.5.2)

At lesser voltages forcing is much weaker: our assessment for 1 V intensity of vibrator input is approximately 5×10^{-4} N. Thus the forcing was always much less than the driving force (spring) $F = 4$ N.

The typical recording of AE with mechanical forcing is shown in Fig. 10.10 and distributions of acoustic emission onsets relative to phases of forcing period T_f at various conditions is shown in Fig. 10.11a, b. Note that at mechanical forcing we have the high order synchronization (HOS) with winding number < 1 (0.01–0.005).

Voltage (and correspondingly, the intensity of mechanical forcing) increase the density of the AE bursts population in certain parts of the forcing period, namely in the first and the last decimals of forcing phase. In between lies a gap or forbidden zone. We suppose that increasing the voltage applied to the vibrator promotes synchronization of AE offsets with external forcing. In case of normal forcing AE activity is maximal at force phases corresponding to minimal oscillating normal stress (phases $0-72^\circ$ and $288-360^\circ$). Slips are absent in the area of maximal normal stress σ_n (phases $102-252^\circ$). A similar pattern is observed for the tangential forcing (Fig. 10.11b, left columns). Such distributions can be expected from the general expression of friction law: $\tau = c + \mu\sigma_n$ in the case of normal forcing as the increase of the normal stress suppresses slip. The slips distribution in the case of tangential forcing reveals the same pattern as at normal forcing. This seems to contradict to the above friction law. The only explanation of this phenomenon is that the real contacting (rubbing) surfaces are not flat. Protuberances of one surface are often sunk into hollows of the opposite surface. That means that both kinds of forcing increase resistance to slip at certain phases of forcing: (1) in the case of strong normal forcing the tip of protuberance is pressed onto bottom of the trough which prevents slip; (2) in the case of strong tangential forcing the edge of the cusp is pressed against the edge of the through and this again prevents slip. Consequently, the slip can be suppressed at the same phases of both kinds of intensive forcing and the optimal condition for slipping are realized in complementary phases of forcing.

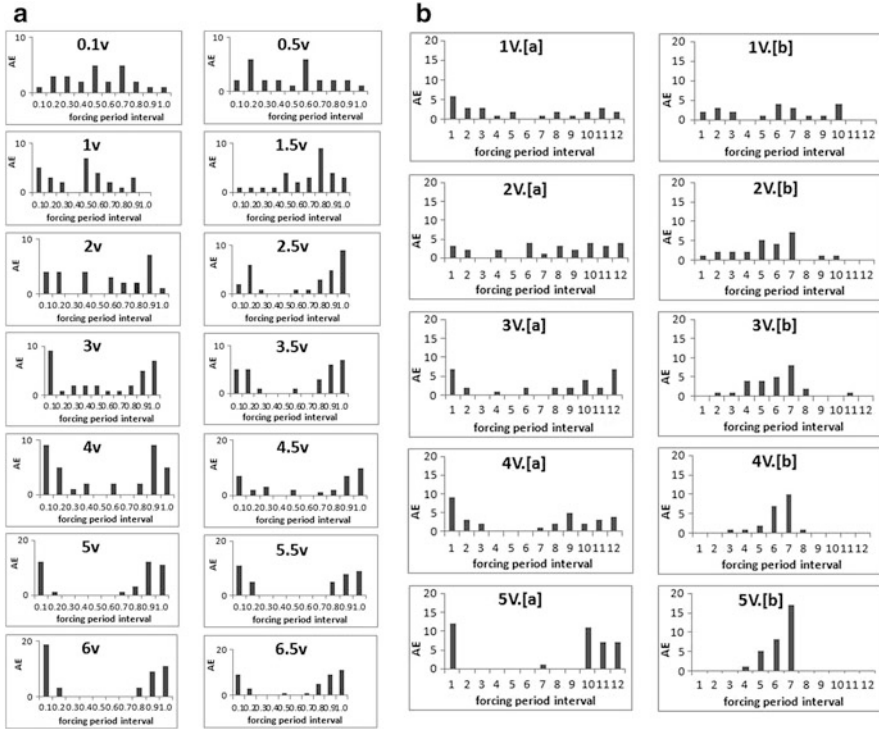


Fig. 10.11 (a) Distribution of acoustic emission onsets relative to phases of forcing period T_f (in decimals of T_f) for different intensities of normal forcing (forcing frequency $f = 20$ Hz). (b) Distribution of AE onsets (the left column) and terminations (the right column) relative to the (mechanical) forcing phase (in twelfths of the forcing period) for different intensities of tangential forcing (forcing frequency of 80 Hz). Clearly, AE events can be synchronized both by the onsets and offsets of the mechanical forcings

Additional arguments on similarity of stick-slip patterns for both kinds of forcing can be deduced from the recent results on the physical mechanism of the stick-slip. According to [91], the slip begins only after rising of the upper (sliding) block over a fixed one to a some height. This means that resistance to both normal and tangential forcings decreases as the area of contacting cusps and troughs decreases. We presume that in the case of periodical forcing this optimal configuration of real rubbing surfaces are observed at certain phases of forcing which are the same for both normal and tangential impact. The similar arguments can be applied to the slip termination distribution (Fig. 10.11b, right columns). Here the phases of optimal termination forcing fill the gap of forbidden phases for onsets (Fig. 10.11b, left columns). In other words termination is promoted at phases forbidden for onsets which seems logical as conditions for terminations and onsets should be mutually exclusive.

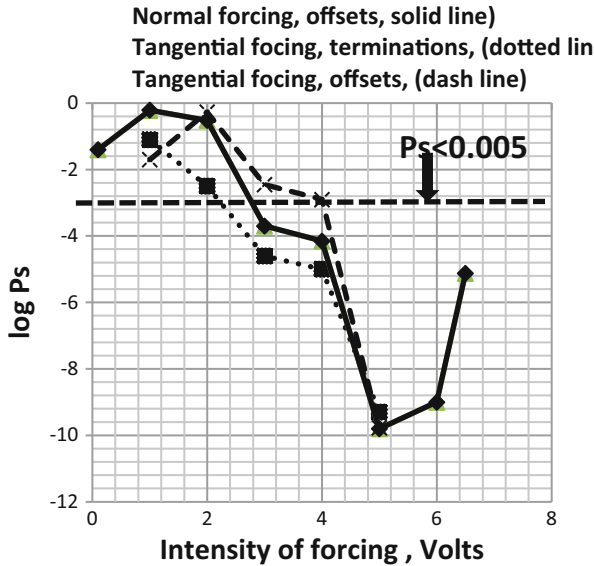


Fig. 10.12 Shuster probability P_s versus mechanical forcing intensity for experimental data (*solid line*—normal forcing offsets, $f = 20$ Hz; *dash line*—tangential forcing offsets, $f = 80$ Hz; *dotted line*—tangential forcing terminations, $f = 80$ Hz). The threshold probability P_s , for which the slips and the forcing are strongly correlated ($P_s < 0.005$) is marked by *horizontal line with arrow*; this means that the probability of random distribution of slips in the area below the line is less than 0.005. Note that at forcing $F \approx 2 \times 10^{-3} N$ (corresponding to the voltage > 4 V) the probability of random distribution of slips is of the order of 10^{-10}

A modified Shuster test [58, 75] was applied to experimental data (namely, to the data for normal forcing offsets, $f = 20$ Hz, tangential forcing offsets, $f = 80$ Hz and tangential forcing terminations, $f = 80$ Hz). Significant “Shuster” probability P_s values indicate that the slips do not occur randomly with respect to the higher forcing intensities (Fig. 10.12). Generally $P_s < 0.05$ is accepted as a reliable threshold, though for confidence we accepted the significance level $P_s < 0.005$; this threshold is shown in Fig. 10.12. Note that at forcing of the order of $10^{-3} N$ (voltage > 4 V) the probability of random distribution of slips is of the order of 10^{-10} . The remarkable detail is also the close similarity of synchronization trends for different forcing modes as well as for both offsets and terminations.

It was a surprise to discover that not only AE onsets can be synchronized by a weak mechanical forcing, but so too can AE offsets at the same coupling strength. This is shown in Fig. 10.11 (right columns) and Fig. 10.12. It is striking that the AE bursts are so well synchronized with mechanical forcing though the waiting interval of AE bursts varies between 100 and 200 periods of forcing. That is, to initiate a single phase-synchronized slip event the forcing oscillator needs to generate enough energy delivered in of hundreds of oscillations to the slider-spring system.

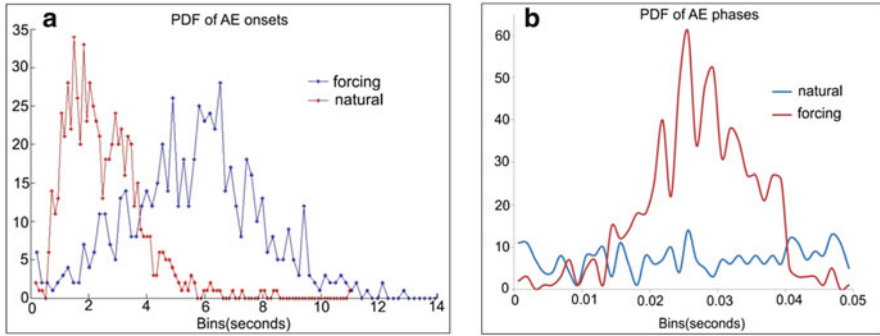


Fig. 10.13 (a) AE waiting time distributions for natural (red line) and forced (blue line) stick-slip in seconds. (b) Distribution of AE phase shifts $\Delta\phi$ relative to the forcing sinusoid phase for natural (blue line) and forced (red line) stick-slip in seconds

AE waiting time (ΔT) distributions for spring stiffness of 235 N and velocity of 0.7 mm/s is shown in Fig. 10.13. The distributions are similar for natural and forced stick-slip except that the mean ΔT is 3.03 and 2.4 s respectively (Fig. 10.13a). This means that forcing shortens waiting times, which is expected from earlier work [90]. In contrast, distributions of phase shifts $\Delta\phi$ between AE and maxima of periodic forcing are quite different for natural and stick-slip forced at 20 Hz (Fig. 10.13b). Of course for natural stick-slip the onsets of AE bursts were compared to maxima of virtual sinusoid with the frequency 20 Hz. There is no preferred $\Delta\phi$ value for the natural stick-slip case, however there is a strong synchronization peak in the $\Delta\phi$ distribution of the forced stick-slip case.

Next we present RPs of series of time intervals between consecutive AE bursts (Fig. 10.14). All RPs in this chapter are plotted using Visual Recurrence Analysis software [88]. These waiting time sequences can be considered as values indicating accumulation of strain energy which is finally released as AEs. Thus within the context of our experimental model, these time interval series can be regarded as proxies to the sequences of “seismic” energy released in consecutive events (seismic rate). In this case we applied a data smoothing procedure similar to what was done for the real seismic processes [34]. Smoothing acts as a low-pass filter and reduces the variability of inter-event times.

We now address RP analysis of AE waiting times and phase shifts $\Delta\phi$ between AEs for natural and forced stick-slip processes as described above. The appropriate delay time and phase space dimension were chosen using MI and FNN approaches respectively. The forcing function was a sinusoidal wave (20 Hz) with a vibration intensity of 4 V. The RPs of AE are shown before (Fig. 10.14a, b) and after (Fig. 10.14c and d) the application of a Savitzky–Golay filter to the AE waiting time (ΔT) data. Although visual inspection hints that the forcing may alter the RP structure (Fig. 10.14a, b), RQA of the short time series showed no difference between the natural and forced stick-slip processes. Smoothing of the original ΔT and $\Delta\phi$ data reveals stronger differences in the two conditions (Fig. 10.14c and d).

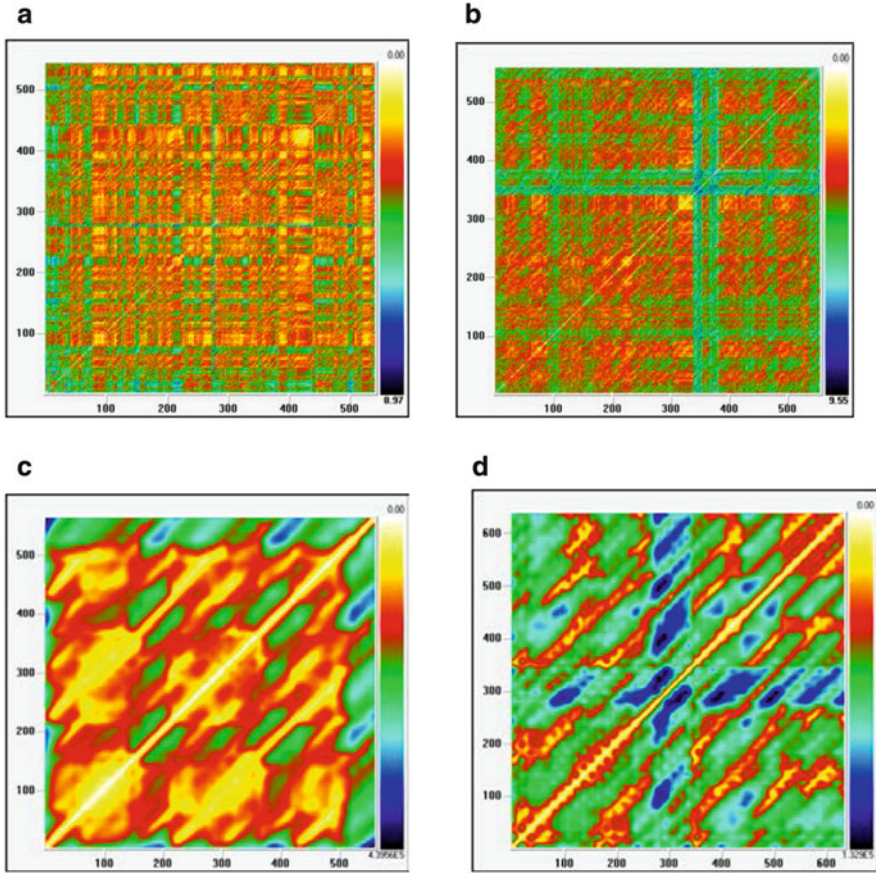


Fig. 10.14 (a) Visual recurrence analysis (VRA) plots of waiting times sequences of acoustic emissions (AE) generated during natural stick-slip (laboratory model of natural seismic process) from original, non-smoothed data. (b) VRA plots of waiting times sequences of AE generated during stick-slip with forcing (laboratory model of forced seismic process). (c) VRA plots for waiting times sequences of AE generated during natural stick-slip smoothed by Savitzky–Golay filter. (d) VRA waiting times sequences of AE generated during stick-slip with forcing smoothed by Savitzky–Golay filter

In any case, it should be noted that in these forced experiments there was high order synchronization with a winding number $n:m \approx 0.2$.

Regarding the phase shifts, RPs of $\Delta\varphi$ are shown before (Fig. 10.15a, b) and after (Fig. 10.15c and d) the application of a Savitzky–Golay filter to the phase shift $\Delta\varphi$ data. The phase delay RPs appear to be more ordered (phase synchronized) under external forcing and this was verified by RQA. For example, compared with the natural stick-slip state, forcings caused increases in both %DET (9 % natural to 28 % forced) and %LAM (12 % natural to 40 % forced) values. Smoothing the data

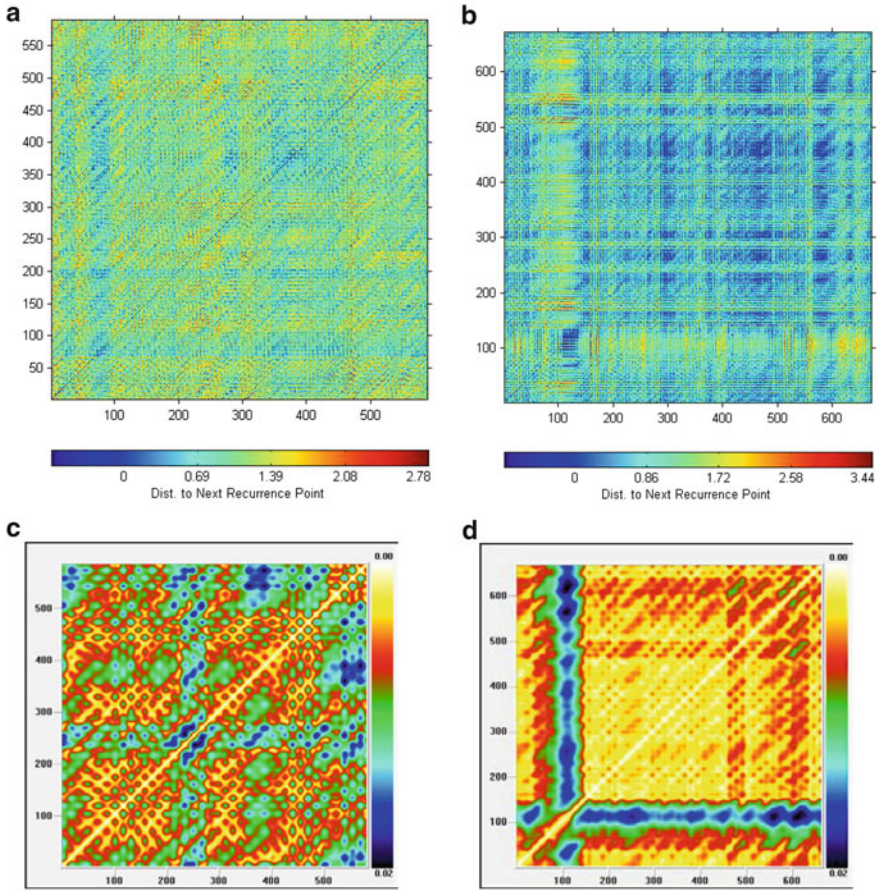


Fig. 10.15 Recurrence plots of time series of phase shift values $\Delta\phi$. (a) RP of phase shifts between onsets of acoustic emission (AE) wave trains generated during natural stick-slip process and maximums of virtual 20 Hz sinusoid. There are no clear recurrent structures. (b) RP of phase shifts between onsets of acoustic emission (AE) wave trains generated during forced stick-slip process and maximums of imposed external periodic forcing (20 Hz). Recurrent structures are more obvious. (c) RP of smoothed by Savitzky–Golay filter time series of phase shifts between onsets of AE bursts during natural stick-slip process and maximums of virtual sinusoid. (d) RP of smoothed by Savitzky–Golay filter time series of phase shifts between onsets of AE bursts and maximums of external periodic forcing (20 Hz) during forced stick-slip process

gave similar results with increases in %DET (67 % natural to 84 % forced), but not %LAM (60 % natural to 62 % forced).

RP plots for original non-smoothed data (Fig. 10.14a, b) contain horizontal and vertical lines/clusters, which means that during both natural and driven stick-slip some states are “laminar.” That is they change slowly or do not change at all during some (integrate, trapping) time interval. These laminar states of AE waiting times

can be compared to the periods of time the upper plate was stuck until the strain from the spring became equal to the friction force.

One important conclusion arises from the HOS data above (Sect. 10.4.4) as pertains to the much discussed interaction between tidal deformation and EQs [11, 74, 75]. That is, in order to uncover tidal effects we should look not only for direct 1:1 correlations between periods and forcings, i.e. for increases/decreases of seismicity exactly at the tidal periods (e.g. 12 h etc.). For EQs, high order phase synchronization can occur at multiples of tidal periods as was shown in laboratory forced stick-slip experiments. It is important to note that phase synchronization of AE or seismic events can be observed irrelative to the duration of event nucleation. Of course, the optimal condition of synchronization (minimal forcing) should correspond to the forcing period which is close to the natural event nucleation time. Additional complication arises from the phenomenon of delay. The phase of response can be shifted quite significantly from the phase of forcing if the last one is weak [82]. Thus the question of tidal forcing of EQs should be reconsidered taking into account these new experimental and theoretical evidences.

10.5 Dynamical Patterns in Seismicity

Analysis of the temporal features of EQ occurrences represents a focus of intensive interdisciplinary research. In this section we study the features of temporal variations of seismicity in the Caucasus Mountains, in general the T/S effects of remote strong earthquakes. We also examine the temporal aspects of seismicity in the areas where natural seismic processes are forced by man-made impacts. The test sites are the high Enguri dam (Georgia) and the magnetohydrodynamic laboratories in Central Asia.

10.5.1 *Recurrence Patterns in Seismic Catalogs*

Matcharashvili et al. [32] presented results of nonlinear analysis of magnitude and waiting time sequences for EQs in the Caucasian region using correlation dimension and algorithmic complexity analyses. It was shown that EQ waiting time series are much more ordered than magnitude sequences. In the present research we used RQA to investigate the complexity of catalogued EQs. Based on the Caucasian EQ catalogue spanning from 1960 to 2011, we investigated the variations in temporal distribution of earthquakes. Daily and monthly occurrences of EQ data sets have been derived both from the original catalogues as well as from declustered catalogues according to the Reasenber algorithm [92, 93] applying a magnitude threshold $M \geq 3.0$. For example, daily and monthly EQ occurrence frequencies are presented for the declustered Caucasian catalogue in Fig. 10.16. From this catalogue we calculated the number of EQ occurrences over consecutive days and months and

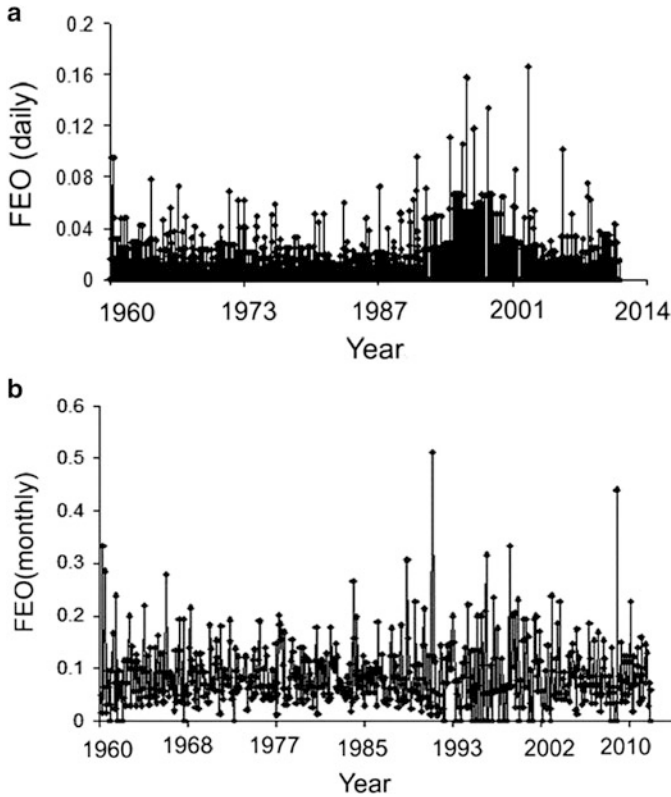


Fig. 10.16 (a) Daily and (b) monthly frequency of EQ occurrences (FEO) vs. years as compiled from the declustered Caucasian EQ catalogue (1960–2011, $M \geq 3.0$)

divided both by the total number of yearly occurrences. These data are identified as frequency of earthquake occurrences (FEO). The daily and monthly FEO series were then normalized to a zero mean and unit variance.

All eight RQA variables were calculated for the daily FEO time series, but here we only report the results for %DET and %LAM calculations. In Fig. 10.17 the results of sliding window RQA calculations are shown for daily FEO values within 1-year windows moved forward in steps of 1-year. There are wide fluctuations in the non-filtered FEO data, but applying the Savitzky–Golay filter smooths the resultant %DET and %LAM values. This filter approximates the data with an n th degree polynomial preserving up to n th moments of the data. Thus, Savitzky–Golay filtering has the advantage over, for instance, a moving average filter since the magnitude of the variations in the data (local extremes) are to a large extent preserved [94].

In order to decrease possible variations caused by the short windows length of 365 days, the same RQA calculations were repeated using a longer window length

Fig. 10.17 (a) Recurrence plots of daily FEO. (b) %DET (black circles) and %LAM (black triangles) of daily frequency of earthquake occurrence time series for 365 days length sliding window and 365 days step. %DET (gray circles) and %LAM (gray triangles) after Savitzky–Golay smoothing

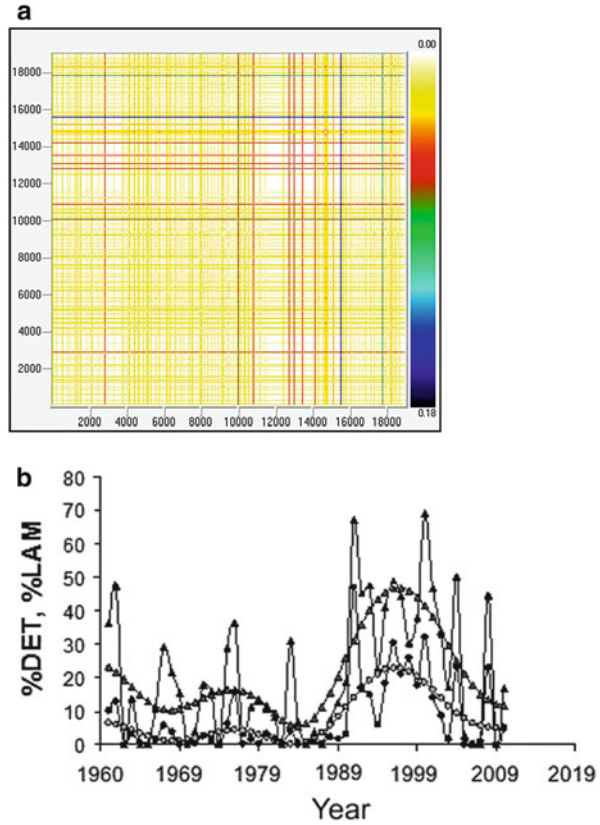
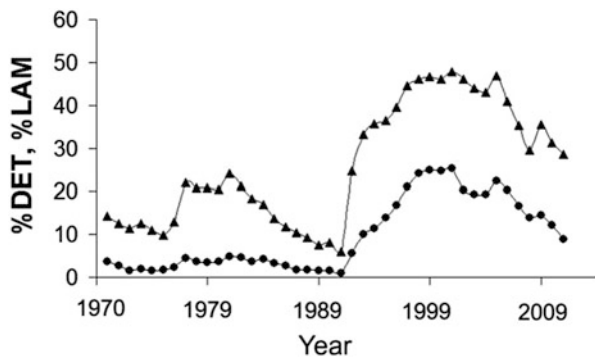


Fig. 10.18 %DET (circles) and %LAM (triangles) of daily frequency of EQ occurrence time series for 3,650 days length sliding window and 365 days step



of 3,650 days on the same 10 year daily FEO data. In these cases increases in %DET and %LAM variables are seen in windows corresponding to the period from 1990 to 2005 (Fig. 10.18).

Results obtained for the monthly FEO data using 10 year windows are shown in Fig. 10.19. These results are similar to those obtained for daily data and indicate that

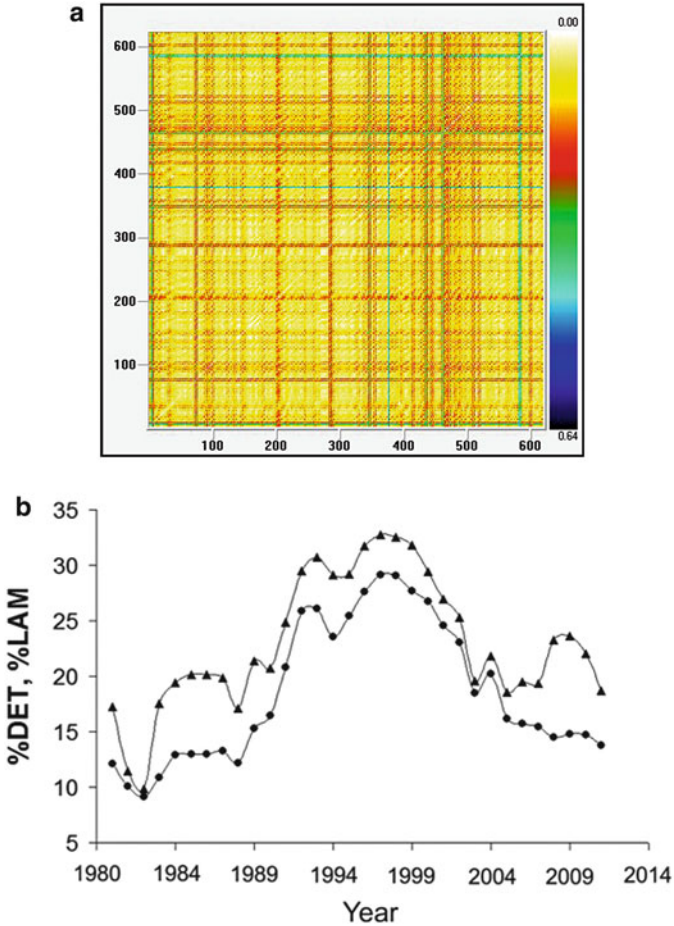
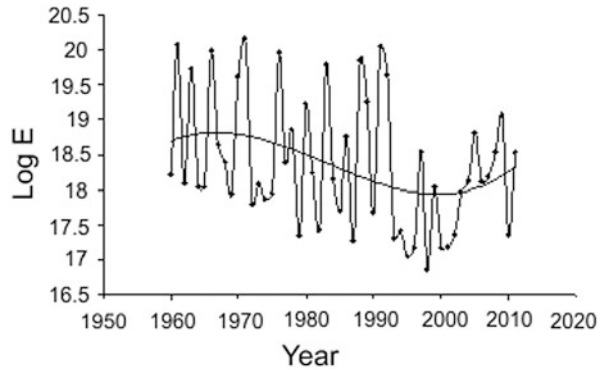


Fig. 10.19 (a) Recurrence plots of FEO. (b) %DET (circles) and %LAM (triangles) of monthly frequency of EQ occurrences for 240 month length sliding window and step of 12 months

the most important changes in temporal structure of considered process (frequency of EQ occurrence) also took place in the time period from approximately 1990 to 2005.

Although in most of the presented RPs above clear regular structures are not discernable qualitatively, it is important to focus on the behaviors of the %DET and %LAM variables which report on quantitative features of EQ occurrences over the years 1990–2005 (Figs. 10.17, 10.18, and 10.19). It should be emphasized that the demonstrated increases in %DET and %LAM measures data coincide with the period of decreased release of seismic energy in the Caucasus Mountains. This is shown in Fig. 10.20.

Fig. 10.20 Yearly release of seismic energy in the Caucasus Mountains (for $M > 3.0$) from 1960 to 2011 as calculated from the declustered catalogue. *Solid curve* is a third order polynomial fit



We hypothesize that the increase in seismic determinism is connected with formation of the “stress shadow” after strong EQs earthquakes of magnitude $M = 6.9$ (Spitak EQ, 1988; Racha EQ, 1991) in the region of Caucasus Mountains [95, 96]. After strong events, tectonic stresses relax (stress shadow appears) meaning that the share of relatively weak, quasi-periodic forces (e.g. tides, seasonal loadings, etc.) increase relative to the main driving tectonic forces. This makes the coupling of these weak forcings with tectonic stresses stronger and renders the time series more ordered (more deterministic).

10.5.2 *Dynamic Triggering and Synchronization of Seismicity*

Finding reliable proofs of seismic T/S dynamics has become possible over last decades due to the accumulation of numerous seismic observations. One kind of dynamic T/S is connected with volcanoes which produce tremors because, unlike EQs, they do not have impulsive onsets. Rather volcanoes present one wave package of long duration without clear arrival times for subsequent waves. Stich et al. [97] reported on swarms of volcanic tremors with periodic occurrences at Deception Island in Antarctica. The characteristic inter-event periods for individual swarms ranged from approximately 10–20 s and were close to integer multiples of the dominant periods of the oceanic microseism (5 s). This evinces synchronization of volcanic tremor activity with the phase of oceanic noise which generates strains in the order of 10^{-7} . It appears that this case is an example of high order synchronization (HOS) of tremor activity with oceanic microseisms (see also Sect. 10.4.4). The 2 s periodicity inside the swarm also looks very similar to our laboratory modeling results (Figs. 10.8 and 10.9).

Another kind of T/S event was discovered over the last several years [12–15, 45, 73, 98, 99]. These so called non-volcanic or tectonic tremors (TT) are connected with activation of local seismic activity by wave trains (mostly Love and Rayleigh waves) from remote yet strong EQs. The TTs are singled out temporal and spatial

correlations of anomalous increases of local seismicity following the remote strong EQ [13]. The peak dynamic values of stress T_p due to the wave trains forcings is very low (of the order of 7–8 kPa) compared to tectonic stresses at the tremor source depth (several MPa). One approach for detecting TTs is to look for any excess seismic activity over the background level in the area in which wave trains arrive from a remote strong EQ. This method should be corrected for artifacts connected with the arrival of strong aftershock wave trains from remote sources. It should be noted that even if wave train stress exceeds the mean triggering threshold TTs are not generated everywhere. This is due to the impact of another important factor, namely, the local (site) strength of Earth material, which is highly heterogeneous. Our intuition is that what matters is not the absolute value of T_p , but the difference between local stress and local strength (failure strength or friction resistance). This is why in some areas with high T_p local seismicity is not triggered and, on the contrary, in some areas TTs are observed even at a low peak stresses. These dynamic differences are due to the competition between stress and strength in the different areas. One of the main factors reducing local strength is the pore pressure of fluids which is within the scope of relatively new field of hydroseismology [100, 101]. Reduced strength can explain high frequency of TTs in hydrothermal areas [45] as high pore pressures reduce the resistance to slip.

Another method of revealing TT seems more reliable. In this case TT events are singled out from the remote strong EQ broadband recording by applying a HF bandpass filter (2–8 Hz). One example of TT is shown in Fig. 10.21. Note that by visual inspection TTs and Love/Rayleigh wave peaks seem to be synchronized. Strict quantitative analysis of synchronization between TT events and wavetrains from remote EQs is very difficult to perform due to: (1) small statistics of tremors (as a rule, several tens of events); and (2) simultaneous forcing by Love (L) and Rayleigh (R) waves. The accepted approach is to compute correlation coefficients between tremor envelopes and L/R waves separately. R/L correlation coefficient ratios can also be computed. Visual analysis of Fig. 10.21 a shows that there is not a one-to-one correspondence between amplitudes of surface waves and tremors. That is, strong tremors occur even in periods of weak forcing and vice versa. It seems that the R and L waves just control (stabilize) one of the unstable periodic orbits of chaotic system (seen here as active fault activation under forcing) resulting quasi-periodic tremors [50].

10.5.3 Phase Synchronization of Seismic Activity Induced by Water Level Variations in Reservoir

It has been documented by many authors that large water reservoirs can cause reservoir-induced seismicity (RIS) [5, 102, 103] or according to a new terminology, reservoir-triggered seismicity (RTS) [104]. The analysis of RTS by nonlinear dynamics methods is of particular interest as the water level change cause

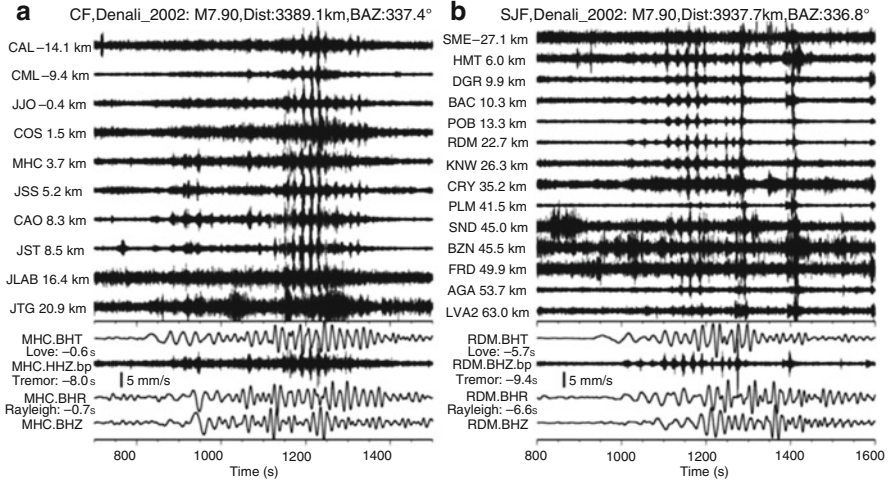


Fig. 10.21 (a) Top: 2–8 Hz band-pass-filtered vertical seismograms showing the move-out of tremor along the Calaveras fault (CF) in northern California (NC) triggered by the 2002 Mw 7.9 Denali fault EQ. The along-strike distance to the tremor source and the station names are marked in the seismograms. The event name and the occurrence year, its magnitude (M), and the epicenter distance (Dist) and back azimuth (BAZ) relative to the broadband station are all shown above the seismograms. *Bottom*: A comparison between the instrument-corrected transverse (BHT), radial (BHR), and vertical (BHZ) velocity seismograms and the 2–8-Hz band-pass-filtered seismogram recorded at the broadband station MHC. The zero time corresponds to the origin time of the main shock. The velocity seismograms have been time-shifted back to the tremor sources. The adjusted times of Love waves, Rayleigh waves and tremor are marked below the station names. The *thick vertical bar* marks the amplitude scale of surface waves. (b) Top: 2–8 Hz band-pass filtered vertical seismograms showing the move-out of tremor triggered by the Denali fault Earthquake along the San Jacinto fault (SJF) in the Anza network in southern California (SC). *Bottom*: A comparison between the velocity and the 2–8 Hz band-pass-filtered seismograms recorded at the broadband station RDM [14]

stress-regime variations in the Earth crust which can be correlated with local seismicity. The 271 m high Enguri Arch dam, still the highest arch dam in operation in the world, was built in the canyon of the Enguri river (West Georgia) in the 1970s. We investigated the change in regional seismic activity around the Enguri reservoir in different periods related to different stress regimes from the natural state (before dam construction) to periodic loading-unloading during the regular exploitation regime [105–107]. Three distinct periods were defined for individual analysis: (1) before impoundment; (2) during flooding and reservoir filling; and (3) during periodic changes of water level.

Figure 10.22 shows the daily record of the water level in the Enguri dam reservoir from 1978 to 1995. Values of the emitted daily seismic energy, as a measure of regional seismic activity, essentially increased at all magnitude scales during the period of territory flooding and reservoir filling. We found that after 8–9 years, the daily seismic energy release fell below those measured before reservoir filling. This

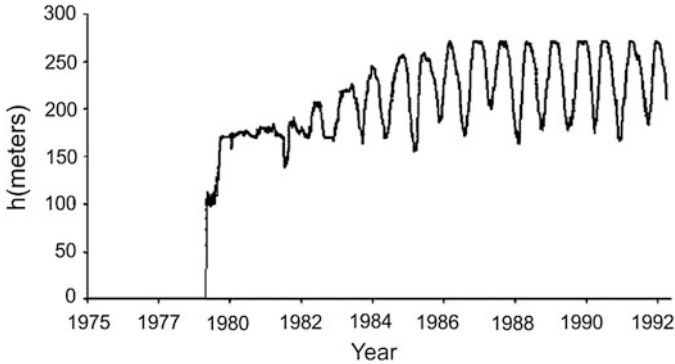


Fig. 10.22 Record of the daily water level height (h) in the lake behind the Enguri Dam versus time from 1975 to 1993

energy release decrease occurred most significantly in the range of large events. The effect of reservoir dynamics is rather small compared to the tectonic stress field. The level of water in the lake changes by 100 m, which means that the pressure at the bottom changes by 10 bar. At a depth of 10 km where the most of hypocenters of EQs are located, the pressure would be much less since the reservoir is of finite volume. For crude assessment of the order of load decrease we used a well-known expression for the stress field increment. Here $\Delta\sigma$ is due to slot-like defects of the size a at the distance r from it: $\Delta\sigma/\sigma \approx (a/r)^{1/2}$ where σ is applied stress, and a is the size of defect. Substituting $\sigma = 10$ bar, $a = 100$ m (here a is the depth of lake) and $r = 10,000$ m (the average depth of hypocenters) we obtain the value of order of 1 bar for $\Delta\sigma$. This is much less than the tectonic stress on this depth, which is of the order of several kilobars.

The period of reservoir filling ended in 1980 and after that, the water level variation became quasi-periodic. We investigated the interevent time (in minutes) of EQ sequences for the whole period, 1960–2012 as shown in Fig. 10.23. Of interest was how variations in reservoir water levels affected temporal features of local seismic activity. We considered both the original and the declustered [92] catalogues applying threshold magnitude of 2.0.

The results are reported as a qualitative RP (Fig. 10.24a) and quantitative, sliding-window RQA (Fig. 10.24b) on the EQ catalogue of the Enguri area for events occurring within 90 km from the location of the dam (1960–2012). It follows from results of EQ magnitude sequences (windows of 1 year repeated in steps of 1 year) that %DET and %LAM both increase after the start of high dam construction and first reservoir impounding (about 1977, Fig. 10.24b). As a caveat it should be emphasized that the first strong increases in the RQA variables may have been caused by engineering explosions during dam construction. These cannot be excluded since the threshold value applied ($M > 2.0$) was relatively low (high sensitivity). Higher threshold values lead to very short data sets disallowing reliable RQA calculations (low sensitivity). At the same time it seems quite logical that

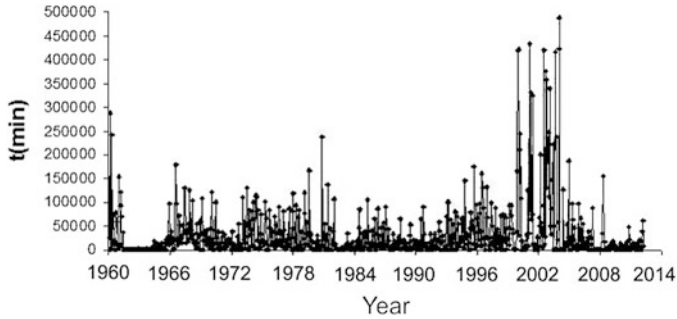


Fig. 10.23 Inter-event time intervals from the original seismic catalogue of Enguri Dam area from 1960 to 2012

increases in %DET and %LAM occurring in the right part of Fig. 10.24b, 10.25 could be explained by the influence of periodic variations of the reservoir water level commencing around 1982.

RQA patterns of earthquake waiting-time distributions also manifest essential temporal changes. As show in Fig. 10.25 the regularity in waiting time series strongly decreases during dam construction and irregular water impoundment and increases during quasiperiodic loading-unloadings of the reservoir. It is interesting to compare %DET of local seismicity waiting times (Fig. 10.25) with our earlier results [107, 108] of %DET of Earth crust tilts time series recorded in the foundation of Enguri Dam for the following periods: (1) long before the reservoir filling; (2) immediately before the start of filling; (3) just after the start of filling, (4) after the second stage of filling; (5) after the third stage of filling; (6) after the fourth stage of filling; and (7) long after the completion of the reservoir filling (Fig. 10.26). There is strong correspondence between %DET tilt patterns and EQ waiting times. We attribute both of these patterns to man-made effects (artifacts). That is, before construction of the dam the high determinism of natural Earth crust dynamics can be due to some regular forcings like tides or seasonal factors. This natural regime was disrupted by construction of dam, but the high determinism was re-established after start of regular load–unload cycles of the reservoir.

The physical mechanism of increased determinism in both EQ waiting times and tilts time series should be due to the periodic load–unload cycles of the reservoir. Arguing in favor of this interpretation are the findings from Singular Spectral Analysis which provides the resultant power spectra of the first four reconstructed components of both the monthly number of earthquakes and the mean water level (see [2]). Thus it was shown that the 1-year periodicity of seismicity in the spectrum correlates well with 1-year water level cycle. Also the weak 4-month period in seismicity can be considered as HOS with the main forcing period of 1-year.

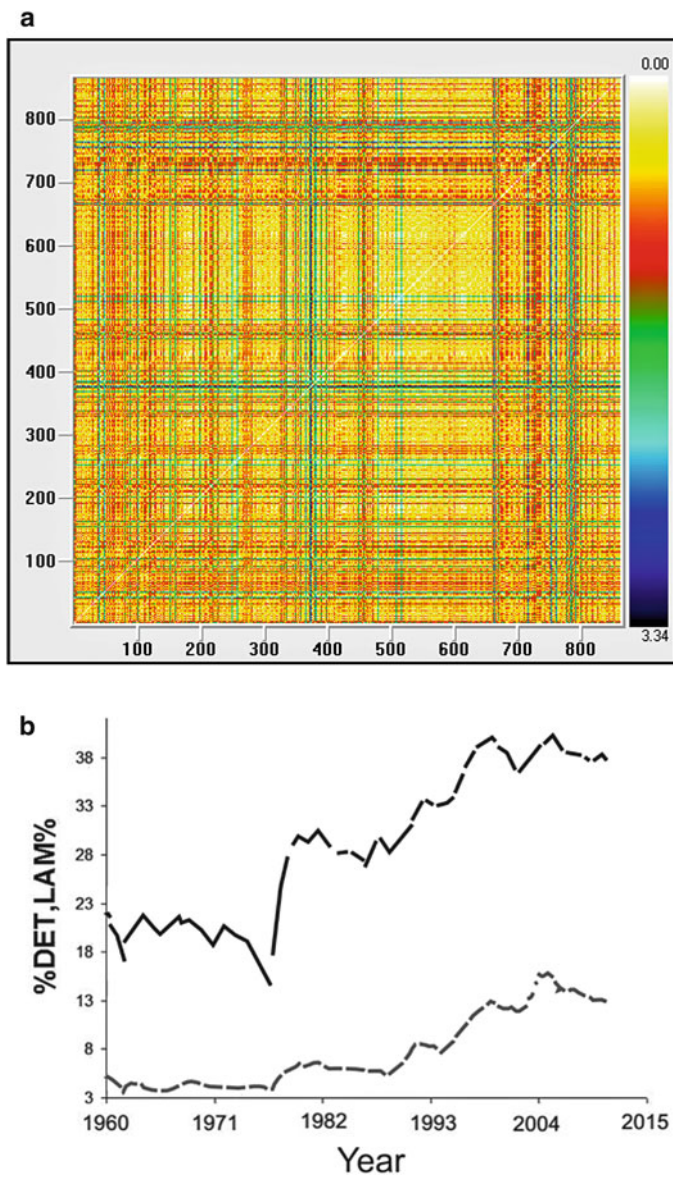


Fig. 10.24 (a) Recurrence plots; (b) %DET (black) and %LAM (grey) of sequence of EQ magnitudes from the Enguri EQ catalogue (1960–2011) at a representative threshold of $M > 2.0$. Window length is 365 days (1 year) with sliding step size of 1 day

Fig. 10.25 %DET (black) and %LAM (gray) of inter-event time sequences from the Enguri EQ catalogue (1960–2011) at a representative threshold of $M > 2.0$. Window length is 365 days (1 year) with sliding step size of 1 day

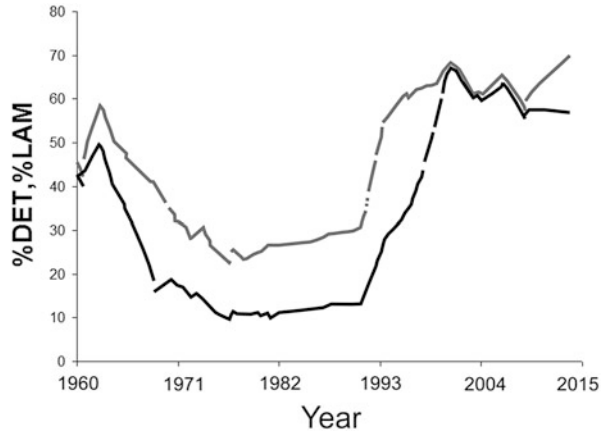
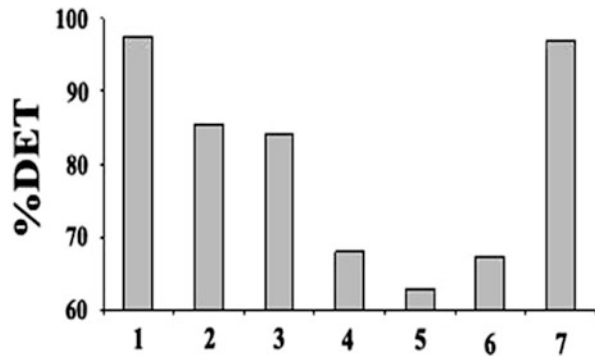


Fig. 10.26 %DET calculated for Earth crust tilt data series for different stages of observation in the foundation of Enguri dam. Numbers on abscissa correspond to periods of observation (see text)



10.5.4 Action of High Energy Electromagnetic Pulses on Local Seismicity

Unique field experiments were carried out by Institute of High Temperatures of Russian Academy of Sciences [9, 10, 109] at Bishkek test area (Central Asia). These studies showed that the actions of high energy electromagnetic pulses radiated by MHD (magnetohydrodynamic) generators or those of sets of batteries cause substantial changes in the number of comparatively small seismic events (energy $K \approx 7$) in the surrounding area with delays of 2–3 days. Laboratory modeling related to these results were considered previously (Sect. 10.4).

The Bishkek area is seismically active as shown in Fig. 10.27. Here are depicted some 14,100 seismic events extracted from the EQ catalogue over two decades. At the test site from January 8, 1983 to March 28, 1990, multiple series of strong current pulses (up to 2.5 kA) were released as 4.5 km long electrical (grounded) dipoles. The energy of separate EM pulses were in the order of $1-2 \cdot 10^7$ J. This is close to energy level of seismic events ($K \approx 7$) which were preferably excited by

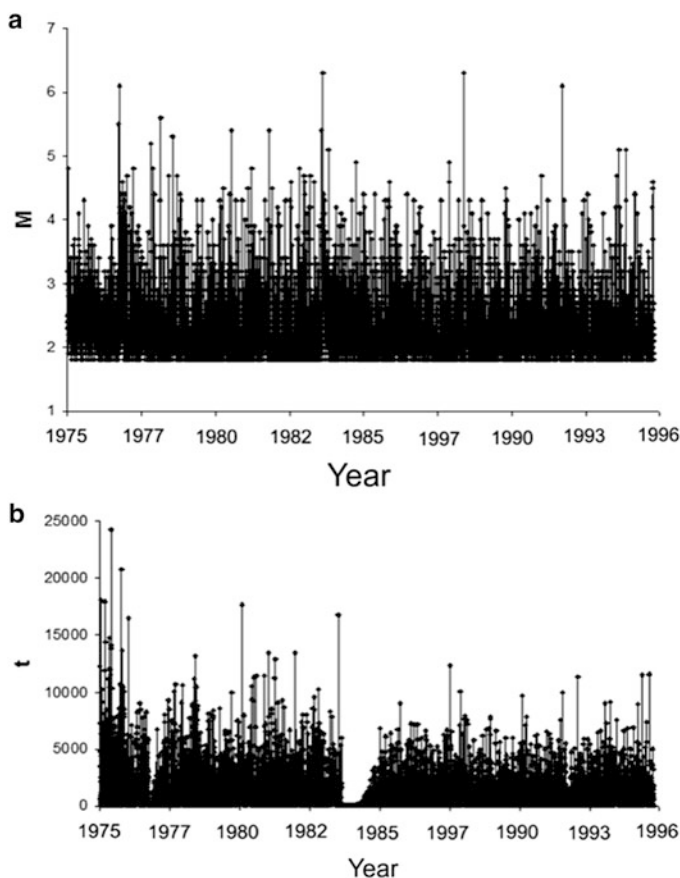


Fig. 10.27 (a) Sequence of EQ magnitudes for threshold $M \geq 1.8$. (b) Inter-event time intervals from the EQ catalogue of Central Asia over the period 1975–1996

injections of EM pulses. Quantitative nonlinear analysis of these data are reported elsewhere [106, 110].

RQA was performed on sequences of EQ waiting times (in minutes) from the Central Asia seismic catalogue which was divided into three parts: (1) 1975–1983 prior to EM experiments; (2) 1983–1990 during EM experiments; and (3) 1988–1996 after termination of EM experiments. The catalogue was tested for completeness [110]. Time intervals between EQs with threshold magnitudes $M > 1.8$ and $M > 2.5$ were investigated.

In Fig. 10.28 %DET and %LAM variables are shown for the waiting time series. Other RQA variables were computed, but are not shown. Using windows with 600 points shifted by 100 points, there are increases in both %DET and %LAM from 1983 to 1986. This time period corresponds to when the EM experiments were carried out and on which the %DET and %LAM calculations were also made.

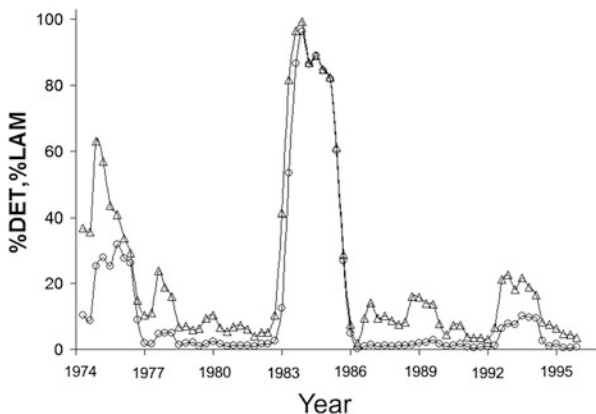


Fig. 10.28 %DET (circles) and %LAM (triangles) of waiting times sequences from the Central Asia EQ catalogue (1975–1996) at a representative threshold $M > 1.8$

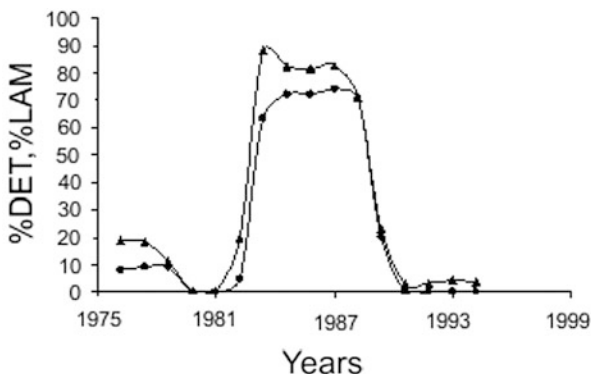


Fig. 10.29 %DET (circles) and %LAM (triangles) of sequence of inter-event times from Central Asia EQ catalogue (1975–1996) at a representative threshold $M > 2.5$. Window length is 500 days with sliding step size of 100 days. *Note:* strong increases in %DET and %LAM during active EM experiments (1983–1988)

%DET and %LAM values of the randomized waiting times sequences were both flat. These results indicate that the original time series had deterministic structuring in both the diagonal and vertical directions.

In order to avoid mistakes due to problems associated with small earthquake registrations at $M > 1.8$, the representative threshold was increased to $M > 2.5$. Results of this analysis are presented in Fig. 10.29. Again observe clear increases in %DET and %LAM between 1983 and 1989 corresponding to the period of active EM experiments. As before, all structures in the original time series were destroyed by randomization of the waiting-time sequence.



Fig. 10.30 %DET (black circles) and %LAM (black triangles) of waiting time sequences from the declustered Central Asia EQ catalogue (1975–1996) at a representative threshold of $M > 2.5$. Window length is 500 days with sliding step size of 100 days. Open symbols correspond to randomized data sets showing attenuation of deterministic structures

Similar increases in %DET and %LAM are also observed for the declustered EQ catalogue as shown in Fig. 10.30. This particular analysis ensures that obtained changes in RQA measures are not caused by aftershocks of strong earthquakes ($M \approx 6.1\text{--}6.3$) that occurred in the periods before, during and after EM soundings.

Figure 10.31 shows recurrence plots of waiting times sequences at Bishkek test area for a complete EQ catalogue (threshold $M \geq 2.5$): (1) before (1975–1983), (2) during (1983–1988), and (3) after performing the EM experiments (1988–1992). Note the compact structuring of RPs during EM experiments.

According to the present (new) RQA results and previous analysis [24, 110] we conclude that strong EM discharges lead to an increased regularity of the temporal distribution of EQs. After cessation of EM experiments the temporal distribution of EQs become more random than before the experiments were conducted. The source of the increased determinism is not quite clear. One explanation can be the presence of several almost regular patterns in the distribution of EM discharge waiting-times.

10.5.5 Geocomplexity Analysis for Earthquake Prediction

The wide variety of new and modern tools for the quantitative analysis of complexity in time series has greatly increased the ability to discover fine variations in seismic and other geophysical time series. Such subtleties are caused by the nonstationarity of underlying processes including anomalies connected with “silent” dynamics prior to strong EQ events [111]. For example, the idea that synchronization phenomena can be correlated with (linked to) closeness of the system to its critical state (EQ manifestation) has been suggested Chelidze et al. [24]. Likewise, systematic exploration of variations of different synchronization characteristics of low-frequency

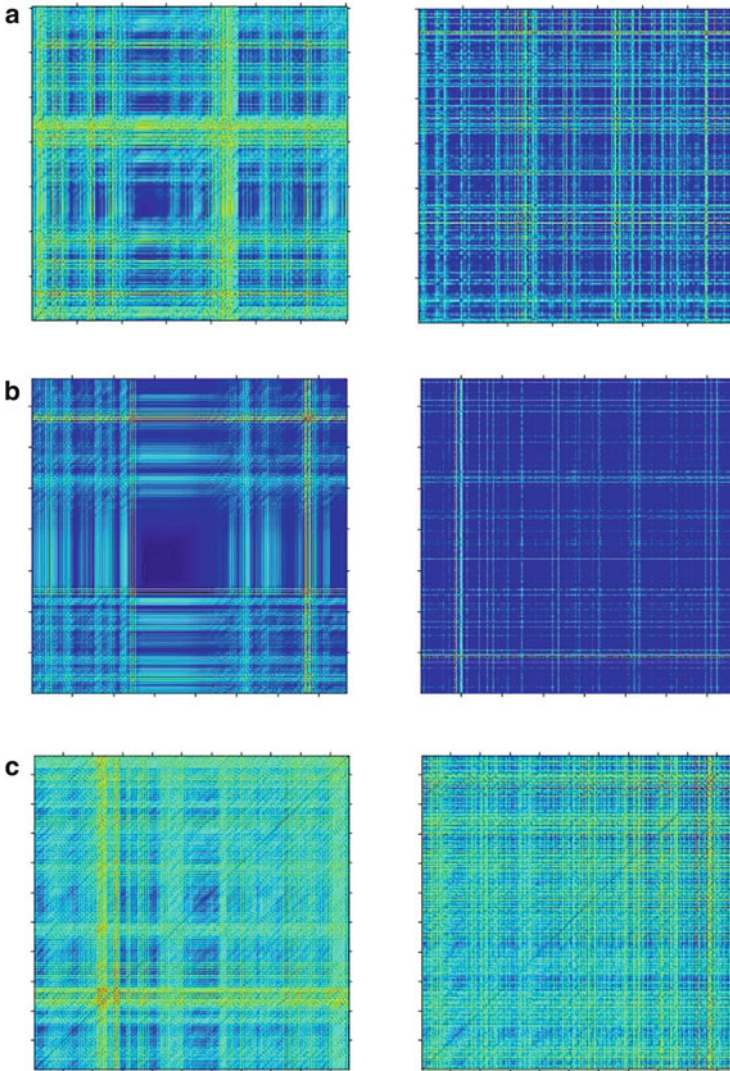


Fig. 10.31 *Left column*: recurrence plots analysis of EQs waiting times sequences at Bishkek test area (complete catalogue, $M \geq 2.5$). **(a)** Before EM experiments (1975–1983), **(b)** during EM experiments (1983–1988), and **(c)** after accomplishing of experiments (1988–1992). *Note*: compact structure in RP during EM experiments. *Right column*: shuffled EQ catalogues for the same three periods

microseismic noise fields obtained during tens of years on the seismic network of Japan have been studied [41]. As a result, several months before great EQ in Japan (Tohoku) on March 11, 2011 ($M = 9$) official predictions on the possibility of strong earthquake in Japan starting from June 2011.

10.6 Conclusions

The dynamic patterns of seismicity for analysis of triggering/synchronization phenomenon were revealed by application of tools from nonlinear dynamics including RQA to various time series: (1) “laboratory” earthquakes measured as acoustic emissions (AEs) during natural stick-slip and stick-slip under weak periodic forcings; (2) regional seismicity of Caucasus Mountains; (3) local seismicity in the area of a large reservoir during its construction and regular exploitation; and (4) local seismicity in Central Asia test area before, during and after the application of strong electric pulses.

For quantitative measuring of synchronization strength several modern tools of nonlinear dynamics were used such as mean effective phase diffusion coefficient, Shannon entropy based characteristic phase synchronization measure, Mutual Information, Recurrence Plots and Recurrence Quantitative Analysis (e.g. percent determinism, %DET and percent laminarity, %LAM, etc.).

The phase synchronization of stick-slip processes induced by a weak electromagnetic or mechanical periodic forcings were investigated on small-scale laboratory experiments. Application of varying frequencies and intensities of forcing allowed for generation of Arnold’s tongue diagrams for EM forcings. It was discovered that not only are the onsets/maxima of AE signals synchronized with forcings, but so too are AE wave train terminations.

The effect of high order synchronization of stick-slip events by weak electromagnetic or mechanical periodic forcings was demonstrated. Two kinds of high order synchronization were discovered: (1) occurrence of one or more AE bursts during a single forcing period; and (2) occurrence of a single AE burst during many forcing periods.

Reviews of recent results of dynamic triggering of local seismicity by remote earthquakes is presented, as well as other examples of triggering/synchronization by reservoir exploitation and strong electromagnetic pulses.

In all these studies from laboratory scale to actual earthquakes, RQA proved to be a very efficient method for revealing deterministic structuring and synchronization in related time series. These results point to the possibility of revealing new fine details in the stick-slip process which can be very useful for refining the understanding of the physical mechanism of frictional motion in general. These findings may also be useful in discovering new but hidden regularities in seismic time series.

Acknowledgments The authors express their gratitude to the Georgian (Rustaveli) National Science Foundation, INTAS foundation and Open Partial Agreement on Major Disasters at Council of Europe (EUR-OPA) for financial support. Authors are grateful for the kind permission of World Scientific and Engineering Academy and Society (WSEAS), Bulletin of Seismological Society of America, Journal of Georgian Geophysical Society and Bulletin of Georgian National Academy of Sciences to reuse Figures from published in these editions papers in the present review. The help of Prof. O. Lursmanashvili, Dr. N. Varamashvili and researchers N. Zhukova, E. Mepharidze and D. Tephnadze is acknowledged.

References

1. D. Broomhead, G. King, On the qualitative analysis of experimental dynamical systems, in *Nonlinear Phenomena and Chaos*, ed. by S. Sarkar (Adam Hilger, Bristol, 1986), pp. 113–144
2. L. Telesca, T. Matcharashvili, T. Chelidze, N. Zhukova, Relationship between seismicity and water level in the Enguri high dam area (Georgia) using the singular spectrum analysis. *Nat. Hazards Earth Syst. Sci.* **12**, 2479–2485 (2012)
3. C.H. Scholz, *Mechanics of Earthquakes and Faulting* (Cambridge University Press, Cambridge, 2003)
4. G. King, Fault interaction, earthquake stress changes and the evolution of seismicity, in *Earthquake Seismology*, volume ed. by H. Kanamori (Elsevier, Amsterdam, 2009), pp. 225–255
5. H.K. Gupta, *Reservoir-Induced Earthquakes* (Elsevier, New York, 1992). 264 pp
6. J.-R. Grasso, D. Sornette, Testing self-organized criticality by induced seismicity. *J. Geophys. Res.* **103**, 29965–29987 (1998)
7. A.V. Nikolaev (ed.), *Induced Seismicity* (“Nauka”, Moscow, 1994) 220 p (in Russian)
8. K. Heki, Snow load and seasonal variation of earthquake occurrence in Japan. *Earth Planet. Sci. Lett.* **207**, 159–164 (2003)
9. N.T. Tarasov, Crustal seismicity variation under electric action. *Trans. (Doklady) Russ. Acad. Sci.* **353A**(3), 445–448 (1997)
10. N. Tarasov, H. Tarasova, A. Avagimov, V. Zeigarnik, The effect of high-power electromagnetic pulses on the seismicity of Central Asia and Kazakhstan. *Volcanol. Seismol. (Moscow)* **N4–5**, 152–160 (1999) (in Russian)
11. C.H. Scholz, Earthquakes: good tidings. *Nature* **425**, 670–671 (2003). doi:[10.1038/425670a](https://doi.org/10.1038/425670a)
12. T. Iwata, Earthquake triggering caused by the external oscillation of stress/strain changes. Community Online Resource for Statistical Seismicity Analysis (2012). doi:[10.5078/corssa-65828518](https://doi.org/10.5078/corssa-65828518). <http://www.corssa.org>
13. D. Hill, S. Prejean, Dynamic triggering, in *Earthquake Seismology*, volume ed. by H. Kanamori (Elsevier, Amsterdam, 2009), pp. 257–293
14. K. Chao, Z. Peng, W. Ch, C.-C. Tang, C.-H. Lin, Remote triggering of non-volcanic tremor around Taiwan. *Geophys. J. Int.* **188**, 301–324 (2012)
15. K. Chao, Z. Peng, A. Fabian, L. Ojha, Comparisons of triggered tremor in California. *Bull. Seismol. Soc. Am.* **102**, 900–908 (2012)
16. R. Meyers (ed.), *Encyclopedia of Complexity and Systems Science* (Springer, New York, 2009)
17. H. Abarbanel, L.S. Tsimring, The analysis of observed chaotic data in physical systems. *Rev. Mod. Phys.* **65**, 1331–1392 (1993)
18. H. Kantz, T. Schreiber, *Nonlinear Time Series Analysis* (Cambridge University Press, Cambridge, 1997)
19. J. Rundle, D. Turcotte, W. Klein (eds.), *Geocomplexity and Physics of Earthquakes* (AGU, Washington, DC, 2009)
20. D. Sornette, *Critical Phenomena in Natural Sciences* (Springer, Heidelberg, 2000)
21. J. Sprott, *Chaos and Time-Series Analysis* (Oxford University Press, Oxford, 2003)
22. S. Strogatz, *Nonlinear Dynamics and Chaos* (Perseus Books Group, Westview, 2000)
23. A. Pikovsky, M.G. Rosenblum, J. Kurths, *Synchronization: Universal Concept in Nonlinear Science* (Cambridge University Press, Cambridge, 2003)
24. T. Chelidze, O. Lursmanashvili, T. Matcharashvili, M. Devidze, Triggering and synchronization of stick slip: waiting times and frequency–energy distribution. *Tectonophysics* **424**, 139–155 (2006)
25. D. Sornette, *Why Stock Markets Crash* (Princeton University Press, Princeton, 2003)
26. A. Bunde, J. Kropp, H. Schellnhuber (eds.), *The Science of Disasters* (Springer, Berlin, 2002)
27. H. Kanamori, E.E. Brodsky, The physics of earthquakes. *Rep. Prog. Phys.* **67**, 1429–1496 (2004)

28. P. Bak, C. Tang, K. Wiesenfeld, Self-organized criticality. *Phys. Rev.* **A38**, 364–374 (1988)
29. Y. Ogata, Statistical models for earthquake occurrences and residual analysis for point processes. *J. Am. Stat. Assoc.* **83**, 9–27 (1988)
30. D. Sornette, M. Werner, Statistical physics approaches to seismicity, in *Encyclopedia of Complexity and Systems Science* (Springer, New York, 2009), pp. 7872–7891
31. C. Goltz, *Fractal and Chaotic Properties of Earthquakes* (Springer, Berlin, 1997)
32. T. Matcharashvili, T. Chelidze, Z. Javakhishvili, Nonlinear analysis of magnitude and interevent time interval sequences for earthquakes of the Caucasian region. *Nonlinear Processes Geophys.* **7**, 9–19 (2000)
33. T. Chelidze, T. Matcharashvili, Complexity of seismic process, measuring and applications – a review. *Tectonophysics* **431**, 49–61 (2007)
34. G. Sobolev, Seismicity dynamics and earthquake predictability. *Nat. Hazards Earth Syst. Sci.* **11**, 445–458 (2011). doi:[10.5194/nhess-11-445-2011](https://doi.org/10.5194/nhess-11-445-2011)
35. T. Rikitake, *Earthquake Forecasting and Warning* (Center for Academic Publications, Tokyo, 1982)
36. K. Mogi, *Earthquake Prediction* (AP, Tokyo, 1985)
37. G.A. Sobolev, A.V. Ponomarev, *Physics of Earthquakes and Precursors* (“Nauka”, Moscow, 2003) (in Russian)
38. R.J. Geller, Earthquake prediction: a critical review. *Geophys. J. Int.* **131**, 425–450 (1997)
39. M. Wyss, D. Booth, The IASPEI procedure for the evaluation of earthquake precursors. *Geophys. J. Int.* **131**, 42–424 (1997)
40. Y. Ogata, K. Katsura, G. Falcone, K. Nanjo, J. Zhuang, Comprehensive and topical evaluations of earthquake forecasts in terms of number, time, space, and magnitude. *Bull. Seismol. Soc. Am.* **103**, 1692–1708 (2013). doi:[10.1785/0120120063](https://doi.org/10.1785/0120120063)
41. A. Lyubushin, Prognostic properties of low-frequency seismic noise. *Nat. Sci.* **4**, 659–666 (2012). doi:[10.4236/ns.2012.428087](https://doi.org/10.4236/ns.2012.428087)
42. D.M. Evans, Denver area earthquakes and the rocky mountain arsenal disposal well. *Mt. Geol.* **3**, 23–26 (1966)
43. S. Hainzl, T. Kraft, J. Wassermann, H. Igel, E. Schmedes, Evidence for rainfall-triggered earthquake activity. *Geophys. Res. Lett.* **33**, L19303 (2006). doi:[10.1029/2006GL027642](https://doi.org/10.1029/2006GL027642)
44. T. Chelidze, T. Matcharashvili, Electromagnetic control of earthquake dynamics? *Comput. Geosci.* **29**, 587–593 (2003)
45. S. Prejean, D. Hill, Dynamic triggering of earthquakes, in *Encyclopedia of Complexity and Systems Science*, ed. by R.A. Meyers (Springer, New York, 2009), pp. 2600–2621
46. S. Boccaletti, C. Grebogi, Y.-C. Lai, H. Mancini, D. Maza, The control of chaos: theory and applications. *Phys. Rep.* **329**, 103–119 (2000)
47. A. Koronovskii, O. Moskalenko, A. Hramov, Mechanisms behind the generalized synchronization conditions. *Tech. Phys.* **51**(2), 143–150 (2006)
48. E. Ott, M. Spano, Controlling chaos. *Phys. Today* **5**, 34–40 (1995)
49. W.L. Ditto, S.N. Rauseo, M.L. Spano, Experimental control of chaos. *Phys. Rev. Lett.* **65**, 3211–3214 (1990)
50. J. Starrett, Control of chaos by occasional bang–bang. *Phys. Rev. E* **67**, 036203, 1–4 (2003)
51. I.I. Blekhman, *Synchronization in Science and Technology* (ASME Press, New York, 1988)
52. M. Palus, Detecting phase synchronization in noisy systems. *Phys. Lett. A* **227**, 301–308 (1997)
53. M. Rosenblum et al., Phase synchronization: from theory to data analysis, in *Handbook of Biological Physics*, ed. by F. Moss, S. Gielen. *Neuro-Informatics*, vol 4 (Elsevier, Amsterdam, 2001), pp. 279–321
54. E. Toledo, M. Rosenblum, J. Kurths, S. Akselrod, Cardiorespiratory synchronization: is it real phenomenon? in *Computers in Cardiology*, ed. by A. Murrey, S. Swiryn (IEEE, Hannover, 1999), pp. 237–240
55. V. Anishchenko, *Dynamical Chaos. Models and Experiments* (World Scientific, Singapore, 1995)

56. C. Tsallis, Possible generalization of Boltzmann–Gibbs statistics. *J. Stat. Phys.* **52**, 479–487 (1988)
57. A. Lempel, J. Ziv, On the complexity of finite sequences. *IEEE Trans. Inf. Theory* **IT-22**, 75–81 (1976)
58. A. Schuster, On lunar and solar periodicities of earthquakes. *Proc. R. Soc. Lond.* **61**, 455–465 (1897)
59. F. Takens, Detecting strange attractors in turbulence, in *Dynamical Systems and Turbulence*, ed. by D.A. Rand, L.S. Young. Springer Lecture Notes in Mathematics, vol. 898 (Springer, Berliner, 1981), pp. 366–381
60. J.-P. Eckmann, S. Kamphorst, D. Ruelle, Recurrence plots of dynamical systems. *Europhys. Lett.* **4**, 973–977 (1987)
61. J.P. Zbilut, C.L. Webber Jr., Embeddings and delays as derived from quantification of recurrence plots. *Phys. Lett. A* **171**, 199–203 (1992)
62. J.P. Zbilut, C. Webber Jr., Detecting deterministic signals in exceptionally noisy environments using cross-recurrence quantization. *Phys. Lett. A* **246**, 122–128 (1998)
63. C.L. Webber Jr., J.P. Zbilut, Recurrence quantification analysis of nonlinear dynamical systems, in *Tutorials in Contemporary Nonlinear Methods for the Behavioral Sciences*, ed. by M.A. Riley, G.C. Van Orden (National Science Foundation, Arlington, VA, 2005), pp. 26–94
64. M. Marwan, Encounters with neighborhood, Ph.D. Thesis. Potsdam, 2003
65. N. Marwan, M. Thiel, N. Nowaczyk, Cross recurrence plot based synchronization of time series. *Nonlinear Processes Geophys.* **9**, 325–331 (2002)
66. N. Marwan, M.C. Romano, M. Thiel, J. Kurths, Recurrence plots for the analysis of complex systems. *Phys. Rep.* **438**, 237–329 (2007)
67. C.L. Webber Jr., N. Marwan, A. Facchini, A. Giuliani, Simpler methods do it better: success of recurrence quantification analysis as a general purpose data analysis tool. *Phys. Lett. A* **373**, 3753–3756 (2009)
68. T. Matcharashvili, T. Chelidze, Nonlinear dynamics as a tool for revealing synchronization and ordering in geophysical time series: application to Caucasus seismicity, in *Synchronization and Triggering: From Fracture to Earthquake Processes*, ed. by V. de Rubeis, Z. Czechowski, R. Teisseyre (Springer, Berlin, 2010), pp. 3–21
69. M. Thiel, M.C. Romano, J. Kurths, R. Meucci, E. Allaria, F.T. Arecchi, Influence of observational noise on the recurrence quantification analysis. *Physica D* **171**, 138–152 (2002)
70. N. Marwan, How to avoid potential pitfalls in recurrence plot based data analysis. *Int. J. Bifurcation Chaos* **21**, 1003–1017 (2011)
71. J.P. Zbilut, J.M. Zaldívar-Comenges, F. Strozzi, Recurrence quantification based Lyapunov exponents for monitoring divergence in experimental data. *Phys. Lett. A* **297**, 173–181 (2002)
72. C.L. Webber Jr., J.P. Zbilut, Dynamical assessment of physiological systems and states using recurrence plot strategies. *J. Appl. Physiol.* **76**, 965–973 (1994)
73. D. Hill, Surface wave potential for triggering tectonic (nonvolcanic) tremor. *Bull. Seismol. Soc. Am.* **100**, 1859–1878 (2010). doi:[10.1785/0120090362](https://doi.org/10.1785/0120090362)
74. N.M. Beeler, D.A. Lockner, Why earthquakes correlate weakly with the solid Earth tides: effects of periodic stress on the rate and probability of earthquake occurrence. *J. Geophys. Res.* **B108**, 2391–2405 (2003)
75. N. Bartlow, D. Lockner, N. Beeler, Laboratory triggering of stick-slip events by oscillatory loading in the presence of pore fluid with implications for physics of tectonic tremor. *J. Geophys. Res.* **117**, B11411 (2012). doi:[10.1029/2012JB009452](https://doi.org/10.1029/2012JB009452)
76. T. Chelidze, T. Matcharashvili, J. Gogiashvili, O. Lursmanashvili, M. Devidze, Phase synchronization of slip in laboratory slider system. *Nonlinear Processes Geophys.* **12** (2005)
77. T. Chelidze, O. Lursmanashvili, T. Matcharashvili, N. Varamashvili, N. Zhukova, E. Mepharidze, Triggering and synchronization of stick-slip: experiments on spring-slider system, in *Synchronization and Triggering: From Fracture to Earthquake Processes*, ed. by V. de Rubeis, Z. Czechowski, R. Teisseyre (Springer, Berlin, 2010), pp. 123–164
78. T. Chelidze, T. Matcharashvili, Triggering and synchronization of seismicity: laboratory and field data – a review, in *Earthquakes – Triggers, Environmental Impact and Potential Hazards*, ed. by K. Konstantinou (Nova Science Pub, New York, 2013), pp. 165–231

79. W.E. Brace, I.D. Byerlee, Stick slip as a mechanism for earthquakes. *Science* **153**, 990–992 (1966)
80. J.H. Dieterich, Modeling of rock friction 1. Experimental results and constitutive equations. *J. Geophys. Res.* **84B**, 2161–2168 (1979)
81. A. Ruina, Slip instability and state variable friction laws. *J. Geophys. Res.* **88B**, 10359–10370 (1983)
82. T. Chelidze, T. Matcharashvili, O. Lursmanashvili, N. Varamashvili, Acoustics of stick-slip deformation under external forcing: the model of seismic process synchronization, in *2nd IASME/WSEAS International Conference on GEOLOGY and SEISMOLOGY (GES '08)* (Cambridge, 2008)
83. T. Chelidze, N. Varamashvili, M. Devidze, Z. Chelidze, V. Chikhladze, T. Matcharashvili, Laboratory study of electromagnetic initiation of slip. *Ann. Geophys.* **45**, 587–599 (2002)
84. T. Chelidze, O. Lursmanashvili, Electromagnetic and mechanical control of slip: laboratory experiments with slider system. *Nonlinear Processes Geophys.* **20**, 1–8 (2003)
85. I. Tamm, *Fundamentals of Theory of Electricity*. 6th Edition (1956) Moscow, State Publishing House of Technical-Theoretical Literature (in Russian)
86. R. Sibson, Crustal stress, faulting and fluid flow, in *Deformation and Fluid Flow Geological Society*, London, Special Publications, vol 78 (1994), pp. 69–84
87. M.G. Rosenblum, A. Pikovsky, J. Kurths, Phase synchronization of chaotic oscillators. *Phys. Rev. Lett.* **76**, 1804–1808 (1996)
88. E. Kononov, Visual Recurrence Analysis (2006), www2.netcom.com/~eugenek/page6.html
89. T. Chelidze, O. Lursmanashvili, T. Matcharashvili, N. Varamashvili, N. Zhukova, E. Mepharidze, High order synchronization of stick-slip process: experiments on spring-slider system. *Nonlinear Dyn.* (2009). doi:[10.1007/s11071-009-9536-6](https://doi.org/10.1007/s11071-009-9536-6)
90. N. Varamashvili, T. Chelidze, O. Lursmanashvili, Phase synchronization of slips by periodical (tangential and normal) mechanical forcing in the spring-slider model. *Acta Geophys.* **56**, 357–371 (2008)
91. O. Ben-David, S. Rubinstein, J. Fineberg, Stick-slip and the evolution of frictional strength. *Nature* **463**, 76–79 (2010). doi:[10.1038/nature08676](https://doi.org/10.1038/nature08676)
92. P. Reasenber, Second-order moment of central California seismicity, 1969–1982. *J. Geophys. Res.* **90**, 5479–5495 (1985)
93. M. Matthews, P. Reasenber, Statistical methods for investigating quiescence and other temporal seismicity patterns. *Pure Appl. Geophys.* **126**, 357–372 (1988)
94. W.H. Press, S.A. Teukolsky, W.T. Vetterling, B.P. Flannery, *Numerical Recipes. The Art of Scientific Computing* (Cambridge University Press, New York, 1997)
95. R.N. Vakarchuk, R.E. Tatevossian, Zh. Ya. Aptekman, V.V. Bykova, The 1991 Racha earthquake, Caucasus. *Izvestiya, Phys. Solid Earth* **49**, 653–659 (2013)
96. G. Sobolev et al., The optical disk “Spitak earthquake of 1988”. *Earthquake Hazard Risk* **6**, 231–238 (1996)
97. D. Stich, J. Almendros, V. Jiménez, F. Mancilla, E. Carmona, Ocean noise triggering of rhythmic long period events at Deception Island volcano. *Geophys. Res. Lett.* **38**, L22307 (2011). doi:[10.1029/2011GL049671](https://doi.org/10.1029/2011GL049671)
98. K. Obara, Nonvolcanic deep tremors associated with subduction in Southwest Japan. *Science* **296**, 1679–1681 (2002)
99. Z. Peng, J.E. Vidale, A.G. Wech, R.M. Nadeau, K.C. Creager, Remote triggering of tremor along the San Andreas fault in central California. *J. Geophys. Res.* **114**, B00A06 (2009). doi:[10.1029/2008JB006049](https://doi.org/10.1029/2008JB006049)
100. C.-J. Wang, M. Manga, Earthquakes and water, in *Lecture Notes in Earth Sciences* (Springer, 2010)
101. J. Costain, J. Bollinger, Review: research results in hydroseismicity from 1987 to 2009. *Bull. Seismol. Soc. Am.* **100**, 1841–1858 (2010). doi:[10.1785/0120090288](https://doi.org/10.1785/0120090288)
102. D. Simpson, Triggered earthquakes. *Ann. Rev. Earth Planetary Sci.* **14**, 21–42 (1986)
103. P. Talwani, On nature of reservoir-induced seismicity. *Pure Appl. Geophys.* **150**, 473–492 (1997)

104. Reservoirs and Seismicity: State of knowledge. Bulletin of International Commission on Large Dams, #137, (Paris, 2011)
105. J. Peinke, T. Matcharashvili, T. Chelidze, J. Gogiashvili, A. Nawroth, O. Lursmanashvili, Z. Javakhishvili, Influence of periodic variations in water level on regional seismic activity around a large reservoir: field data and laboratory model. *Phys. Earth Plan. Interiors* **156**, 130–142 (2006)
106. T. Chelidze, V. de Rubeis, T. Matcharashvili, P. Tosi, Dynamical changes induced by strong electromagnetic discharges in earthquakes' waiting time distribution at the Bishkek Test Area (Central Asia), in *Synchronization and Triggering: From Fracture to Earthquake Processes*, ed. by V. de Rubeis, Z. Czechowski, R. Teisseyre (Springer, Berlin, 2010), pp. 339–360
107. T. Matcharashvili, T. Chelidze, V. Abashidze, N. Zhukova, E. Meparidze, Changes in dynamics of seismic processes around Enguri high dam reservoir induced by periodic variation of water level, in *Synchronization and Triggering: From Fracture to Earthquake Processes*, ed. by V. de Rubeis, Z. Czechowski, R. Teisseyre (Springer, Berlin, 2010), pp. 273–286
108. T. Matcharashvili, T. Chelidze, V. Abashidze, N. Zhukova, E. Meparidze, Evidence for changes in the dynamics of Earth crust tilts caused by the large dam construction and reservoir filling at the Enguri dam international test area (Georgia). *Nonlinear Dyn.* (2011). doi:[10.1007/s11071-010-9930-0](https://doi.org/10.1007/s11071-010-9930-0)
109. N. Jones, The quake machine. *New Scientists*. June 30 (2001), 2297, pp. 34–37
110. T. Chelidze, V. De Rubeis, T. Matcharashvili, P. Tosi, Influence of electro magnetic strong discharges on the dynamics of earthquakes time distribution at the Bishkek test area. *Ann. Geophys.* **49**, 989–1000 (2006)
111. V. Keilis-Boirok, A. Gabrielov, A. Soloviev, Geocomplexity and earthquake prediction, in *Encyclopedia of Complexity and System Science*, ed. by R. Meyers (Springer, New York, 2009), pp. 4178–4194